# WIND TUNNEL STUDIES TO MITIGATE SNOWDRIFT INTO ROOFTOP AIR-HANDLING COURTS ON UNIVERSITY OF COLORADO HEALTH SCIENCES CENTER



Prepared by

Thomas Z. Tan*

Robert N. Meroney+

Final Report

for

Physical Plant and Maintenance Department

University of Colorado Health Sciences Center

Denver, Colorado 80262

* Research Associate

+ Professor, Civil Engineering

FLUID MECHANICS AND WIND ENGINEERING PROGRAM

Colorado State University

CSU Contract No. 2-97850

CER88-89TZT-RNM-15

# WIND TUNNEL STUDIES TO MITIGATE SNOWDRIFT INTO ROOFTOP AIR-HANDLING COURTS ON UNIVERSITY OF COLORADO HEALTH SCIENCES CENTER

FINAL REPORT

(May 1989 - July 1989)

Prepared by

Thomas Z. Tan*
Robert N. Meroney+

for

Physical Plant and Maintenance Department
University of Colorado Health Sciences Center
Denver, Colorado 80262

* Research Associate
+ Professor, Civil Engineering

Colorado State University

CSU Contract No. 2-97850
CER88-89TZT-RNM-15

**ACKNOWLEDGEMENTS**

The authors wish to express their gratitude to the staff and personnel of the Fluid Dynamics and Diffusion Laboratory at Colorado State University. Special thanks go to Mr. Q. Roberts and Mr. D. Parce who built the 1:50 scale model, and Mr. D. Parce and Mr. O. Saad who assisted during flow visualization and snowdrift data acquisition.

**ABSTRACT**

WIND TUNNEL STUDIES TO MITIGATE SNOWDRIFT INTO ROOFTOP
AIR-HANDLING COURTS ON UNIVERSITY OF COLORADO HEALTH SCIENCES CENTER

A wind-tunnel measurement program was performed to study the effectiveness of snow fences, diversion walls, canopies and flat roofs for sheltering the air handling courts on the penthouse roof of the University of Colorado Health Sciences Center (UCHSC) from snow entrainment. The measurement program used smoke visualization and snow simulant pattern observations to identify favorable combinations and locations for various canopies, fences and shelters which appear to reduce snow capture by into the air-handling courts.

TABLE OF CONTENTS

## LIST OF TABLES

## LIST OF FIGURES

## LIST OF SYMBOLS

| | |
|---|---|
| A,B,C | Constants |
| $C_p$ | Specific heat capacity at constant pressure |
| $C_D$ | Drag coefficient |
| E | Hot wire voltage output |
| h | Height of the obstacle |
| g | Gravitational acceleration |
| k | Von Karman constant, equal to 0.4 |
| L | Length |
| $L_m$ | Model length |
| $L_p$ | Prototype length |
| $L_{mo}$ | Monin-Obukhov stability length |
| Q | Flow rate |
| $Q_m$ | Model flow rate |
| $Q_p$ | Prototype flow rate |
| S | Distance downstream of the obstacle |
| T | Temperature |
| U,V,u,v | Velocity |
| $U_*$ | Friction velocity |
| $U_{*t}$ | Threshold velocity |
| $U_m$ | Model wind velocity |
| $U_p$ | Prototype wind velocity |
| $U_{ref}$ | Reference wind velocity |
| x | Distance |
| z | Height above ground |
| $z_o$ | Roughness length |

Greek Characters

| | |
|---|---|
| $\Gamma$ | Adiabatic potential temperature lapse rate |
| $\kappa$ | Thermal conductivity |
| $\mu$ | Dynamic viscosity |
| $\nu$ | Kinematic viscosity |
| $\rho$ | Density |
| $\chi$ | Mole or volume fraction of a gas component |
| $\Omega$ | Angular velocity of earth - $0.726*10^{-4}$ rad/s |

General Dimensionless Parameters

| | |
|---|---|
| Ec | Eckert number |
| Ma | Mach number |
| Re | Reynolds number |
| Ri | Bulk Richardson number |
| Ro | Rossby number |
| Pr | Prandtl number |
| $V$ | Volume flux ratio ($Q/U_H L^2$) |

Snow Simulation Criteria

| | | |
|---|---|---|
| 1. | $D_p/L$ | Particle diameter - length ratio |
| 2. | $U(h)/U_f$ | Reference to particle terminal speed ratio |
| 3. | $[U(h)]^2/gL$ | Froude number |
| 4. | e | Coefficient of restitution |
| 5. | $L_m/L_p$ | Topographic geometric similarity |
| 6. | $z_o/L$ | Roughness similitude |
| 7. | $z_o'/L$ | Roughness similitude in saltation |
| 8. | $h/L$ | Reference height ratio |
| 9. | $z_o/L^*$ | Stability parameter |
| 10. | $\lambda/L$ | Ripple length ratio |
| 11. | $U_f/U_{*t}$ | Particle property similitude |
| 12. | $U_{*t}D_p/\nu$ | Particle friction Reynolds number |
| 13. | $U(h)L/\nu$ | Flow Reynolds number |
| 14. | $U_*/U_{*t}$ | Friction speed ratio |
| 15. | $\rho/\rho_p$ | Density ratio |
| 16. | $U(h)t/L$ | Time scale |

# 1 INTRODUCTION

The Physical Plant and Maintenance Department, University of Colorado Health Sciences Center (UCHSC), must plan for adequate ventilation of the School of Medicine. Ventilation and air handling units housing the fans and ancillary equipment, air intakes and exhaust vents are located in the 6th Floor Penthouse Mechanical Room.

A serious problem exists concerning the current operation of the UCHSC ventilation system. First, during snowstorms snow drifts from the roof into the air-handling courts. The snow pile-up blocks the filters in the air handling units and impedes the passage of air. Negative pressures produced inside the air-handling units can result in unit collapse; whereas, temporary by-passing the units by opening the access doors in the air handling units results in recirculation of air and odors throughout the School of Medicine.

The objectives of the model tests requested by UCHSC are:

a) To determine the effectiveness of alternative snow fence and deflector arrangements on accumulation of snow within the courts,

b) To determine the effectiveness of various geometry canopies on accumulation of snow within the courts, and

c) To recommend an optimum structural arrangement of fences, deflectors, or canopies.

These objectives were carried out for a series of tests oriented on the penthouse roof of the Mechanical Room. Tests were performed in two test groups:

Group 1A: Smoke visualization tests of air flow around and over the UCHSC, and

Group 1B: Snow simulant visualization of deposition and movement over the penthouse roof of the UCHSC which will determine the effectiveness of different configurations of snow fences, canopies and flat roofs to shelter the air-handling courts on the penthouse roof of UCHSC.

Figure 1 provides a top view of the UCHSC and other surrounding buildings.

This report deals only with the Group 1 study.

# 2 TECHNICAL DISCUSSION ON WIND-TUNNEL MODELING

The Appendix summarizes the current status of understanding for snow movement, obstacle and terrain aerodynamics and physical simulation of these flows. Currently there is no numerical program capable of producing the necessary flow deflection/snow deposition information. Wind-tunnel modeling can simulate the dominant snow movement mechanisms and produce reasonable estimates of the influence of ventilator air flow, building interference, and site effects on snow deposition. A series of fluid-modeling experiments were conducted in response to the UCHSC inquiry which should provide information about the impact of various structures on snow movement.

Laboratory measurement techniques are discussed in this section, along with methods used to convert measured model quantities to their meaningful field equivalents. Some of the methods used are conventional and need little elaboration.

For snow situations such as are anticipated for the roof of the UCHSC building, alternative roof configurations were examined in a wind tunnel. All the tests used borax as a snow simulant (white, granulated, nearly correct density, and fall velocity) in a meteorological wind tunnel adjusted to produce simulated wind profiles and turbulent eddies of the correct scale with respect to the UCHSC model. The alternative configurations were ranked in order of effectiveness.

## 2.1 Wind Tunnel and Model Arrangement

### 2.1.1 *Wind Tunnel Arrangement and Model Scales*

The experiments were performed in the Environmental Wind Tunnel (EWT) shown in Figure 2. This wind tunnel, especially designed to study atmospheric flow phenomena, incorporates special features such as an adjustable ceiling, a rotating turntable and a long test section to permit adequate reproduction of micrometeorological behavior. Mean wind speeds of 0.1 to 15 m/sec in the EWT can be obtained. Boundary-layer thickness up to 1.2 m can be developed "naturally" over the downstream 6 m of the EWT test section by using vortex generators at the test section entrance and surface roughness on the floor. The flexible test section on the EWT roof is adjustable in height to permit the longitudinal pressure gradient to be set at zero.

A model scale of 1:50 was chosen to simulated the roof and penthouse of the UCHSC. Only the upper floors were modeled since the kinematics of the snow were expected to be dominated by roof top features such as parapets, satellite dish, and roof-top access structures. A large model scale was chosen to maximize experimental resolution.

Since the 1:50 scale model produced a blockage percentage equal to 7.1%, the Environmental Wind Tunnel Ceiling was adjusted upward 15 cm to reduce blockage and minimize longitudinal pressure gradients over the structure.

### 2.1.2 *Model Intake Simulation*

There are two air-handling courts on the roof top of the medical building. The intake air flow rates were scaled down according to the simulation laws. The dimensionless volume flux ratio is

$$(Q/UL^2)_{model} = (Q/UL^2)_{prototype}$$

The length scale was chosen to be 1:50. The model to field velocity ratio should be equal to the friction velocity ratio, which was set equal to the threshold velocity ratio (Anno, 1985)

$$U_m/U_p = U_{*m}/U_{*p} = U_{*tm}/U_{*tp}.$$

Borax particles behave similarly to snow particles; thus, the threshold velocity ratio may be assumed equal to one, which means that the

$$U_m/U_p = U_{*m}/U_{*p} = 1$$

This implies that the intake air flow rates can be scaled as

$$Q_m/Q_p = (L_m/L_p)^2$$

Table 3 shows the field and the model intake air flow rates for each intake area. The intake flow rates were simulated by using three shop-vacuum cleaners adjusted to the appropriate suction conditions by variacs.

### 2.1.3 *Barrier and Canopy Configurations*

Sixteen different configurations of barriers, fences and canopies were examined in an effort to identify an optimum snow control strategy.

Three solid barrier arrangements were examined: Solid A (Figure 3), Solid B (Figure 4) and Solid C (Figure 5). All the solid barriers had the same height of 1.2 in, which is equivalent to 5 ft in the field.

Fences with 50% porosity were also evaluated for different locations on top of the roof. There were four configurations: Fence A (Figure 6), Fence B (Figure 7), Fence C (Figure 8) and Fence D (Figure 9). The fences also had a uniform height of 1.2 in.

Five kinds of canopies were studied: A pitched roof Canopy A (Figure 10), which could be adjusted to two different heights to form

Canopy D (the height is 0.6 in of model scale and 2.5 ft of prototype) and Canopy E (the height is 1.8 in, equivalent to 7.5 ft of prototype), and also roof with extended overhanging eaves Canopy B (Figure 11) and Canopy C (Figure 12).

One combination of canopy and solid barrier and one combination of canopy and fence were tested. The first case was referred to as Combine A (Figure 13) while the second case was referred to as Combine B (Figure 14).

Finally, two additional configurations were examined by covering the intake areas with flat roofs with overhangs on all four edges (Figure 15), and the flat roofs with a half roof height solid barrier under the roofs along the intake edges (Figure 16).

## 2.2 Wind Velocity Profile

Approach flow wind conditions were sought in the wind tunnel which replicate typical urban velocity profile and turbulence conditions. Considering the presence of the surrounding hospital complex a turbulence level of 15-20% was selected as appropriate.

### 2.2.1 *Wind Profile Measurement*

Velocity measurements were made with single-hot-film probes and anemometry equipment manufactured by Thermo-System, Inc. (TSI).

**Velocity Standard**

The velocity standard used in the present study consisted of a Matheson Model 8116-0154 mass flowmeter and a profile conditioning section designed and calibrated by the Fluid Dynamics and Diffusion (FDDL) staff at Colorado State University (CSU). The mass flowmeter measures mass flow rate independent of temperature and pressure. The profile conditioning section forms a flat velocity profile of very low turbulence at the position where the hot-film-probe is located. Incorporating a measurement of the ambient atmospheric pressure, temperature and a profile correction factor permits the calibration of velocity at the measurement station from 0.15-2.2 m/s to within ± 5 percent.

**Single-Hot-Film Probe Measurements**

Single-hot-film (TSI 1210 Sensor) measurements were used to document the longitudinal turbulence levels for the approach flow conditions. During calibration the probe voltages were recorded at several velocities covering the range of interest. These voltage-velocity (E,U) pairs were then regressed to the equation $E^2 = A + BU^c$ via the least squares approach for various assumed values of the exponent c. Convergence to the minimum

residual error was accelerated by using the secant method to find the best new estimate for the exponent c.

The hot-film-probe was mounted on a vertical traverse and positioned over the measurement location in the wind tunnel. The anemometer's output voltage was digitized and stored within an IBM AT computer. This voltage time series was converted to a velocity time series using the inverse of the calibration equation; $U = [(E^2 - A)/B]^{1/c}$. The velocity time series was then analyzed for pertinent statistical quantities, such as mean velocity and root-mean-square turbulent velocity fluctuations. The computer system would move the velocity probe to a vertical position, acquire the data, then move on to the next vertical positions, thus obtaining an entire vertical velocity profile automatically.

**Error Statement**

The calibration curve yielded hot film anemometer velocities that were always within 2 percent of the known calibrator velocity. Considering the accumulative effect of calibrator, calibration curve fit and other errors the model velocity time series should be accurate to within 10 percent.

Table 1 shows the calibration data for hot-wire used for this experiment. The calibration error is within 0.4 percent as indicated. The accumulative errors in this case are believed within 5 percent.

### 2.2.2 *The Relation between Velocity Profiles for Two Scale Models*

Similitude of air movement about buildings requires that the velocity and turbulence intensity profiles are matched at equvalent heights. However, since this study emphasizes roof top air movements, only the rate of change with height of wind speed and turbulence at roof top levels are significant. A scaled model approach wind profile was sought such that:

$$(\partial u/\partial z)_{prototype} = (\partial u/\partial z)_{model}, \text{ and}$$

$$(u'/\bar{u})_{prototype} = (u'/\bar{u})_{model}.$$

The horizontal air speed within the logarithmic portion of the boundary layer holds as

$$u/u_{ref} = u_*/(u_{ref}*k)\ \ln(z/z_o),$$

By taking derivatives for both $z_1$ and $z_2$, where $z_1$ is prototype roof height and $z_2$ is the prototype roof height of 1:50 scal model.

$$(u_*/u_{ref})_1\ 1/z_1 = (u_*/u_{ref})_2\ 1/z_2$$

According to Sutton (1953) (pg.257),

$$C_D^{1/2} = u_*/u_{ref} = 1.41*k/\ln[(z+z_o)/z_o]$$

This gives

$$\ln[(z_1+z_{o1})/z_{o1}] = \ln[(z_2+z_{o2})/z_{o2}]*(z_2/z_1)$$

or

$$(z_1+z_{o1})/z_{o1} = [(z_2+z_{o2})/z_{o2}]^{(z_2/z_1)}$$

Here $z_o$ can be ignored compared to $z_1$ and $z_2$, which leads to the relationship between $z_{o1}$ and $z_{o2}$

$$z_{o2} = z_2*(z_{o1}/z_1)^{(z_1/z_2)}.$$

By giving an example, if

$$z_1 = 71 \text{ m}$$

$$z_2 = 24 \text{ m}$$

$$z_{o1} = 35 \text{ cm}$$

then

$$z_{o2} = 3.59*10^{-6} \text{ m}$$

From the fact that $z_{o2}$ is close to zero, it can be concluded that no boundary layer is necessary for the top half of the model Medical Health Center building. But the turbulence intensity at $Z_2$ should be maintained the same as the one at $Z_1$.

### 2.2.3 *Velocity Profile for 1:50 Scale Model*

In this model study a nearly uniform velocity profile at roof levels was sought as a result of above discussion. The turbulence intensity was maintained at a typical suburban scale.

The uniform and high turbulence flow was achieved by the combination of spires at the entrance of the wind tunnel, a 7.5 in high barrier 9 ft from the spires and a cross bar grid 15 ft downstream from the barrier.

Table 2 summarizes the velocity and turbulence data measured over the site of the model. Figure 17 and Figure 18 show the velocity profile and the turbulence profile.

## 2.3 Flow Visualization Techniques

A visible plume was produced by passing the simulant gas, whose flow rate was controlled by the mass flow meter, through a smoke generator (Fog/Smoke Machine manufactured by Roscolab, Ltd.). The smoke was directed through tygon tubing to different locations upwind around the model. The visible plumes for each test were recorded on VHS video cassettes with a Panasonic Omnivision II camera/recorder system. Run number titles were placed on the video cassette with a title generator. Numerous views were taken for different orientations and canopy configurations.

Figure 19 shows the smoke being directed toward the intake wells without additional protection. Figure 20 shows typical smoke patterns downstream of a solid barrier configuration. Figure 21 shows the smoke with other fence and canopy configurations.

A complete set of 35mm slides and television recordings have been provided to the sponsor.

## 2.4 Snowdrift Measurement Techniques

Snow storms were simulated by using a modified fertilizer spreader (Model CB1000 manufactured by Cyclone), whose speed was controlled by a AC motor through a variac. There was a feeder opening underneath the hopper of the spreader, which could be adjusted by a lever arm by means of the guide bracket(Figure 22). By adjusting the AC motor and the lever arm, the snow fall rate was controlled.

The spreader was set upstream in order to let the falling "snow" cover the entire roof area. By opening the feeder at the bottom of the hopper for two minutes, a snow storm lasting for an equal period was generated for each simulating study. From the assumption that the model wind speed is equal to the field speed (Section 2.1.2), the time factor is equal to the length scale factor, that is the time factor is 1:50. This implies that 2 minutes of modeling time is equal to 1 hour and 40 minutes of field snow storm period. The video camera taped the entire two minute period of snow fall for each run.

The final snow pattern on the roof top was also recorded on either color slide or black-white negative. The amount of simulant snow which fell into each ventilation well was weighed separately. Finally, a vacuum cleaner was used to remove all the borax from the roof top before the next test.

Figure 23 shows the spreader and the model inside the Environmental Wind Tunnel. Figure 24, Figure 25 and Figure 26 show typical snow patterns on the roof of the UCMHC under different shelter configurations.

# 3 RESULTS AND DISCUSSIONS

The wind tunnel tests described in Chapter 2 were performed to identify an optimum roo-top shelter arrangement to protect air-hangler courts from snow blockage. Differentiation between various alternatives were based on the collective examination of smoke visualization, snow simulant visualization, and snow accumulation measurements within the air-handler wells.

## 3.1 Visualization Results

Table 4 lists all the visualization runs performed during this project. A 1/2" VHS television tape was provided separately to the sponsor.

A total of 68 smoke test cases were performed to evaluate the effectiveness of various fence, canopy and flat roof configurations for minimizing the amount of smoke drawn into the ventilation wells. The tests were grouped by configuration in a progressive order of wind orientation.

Examination of the visual records of these experiments revealed the following:

**a) Vacuum Intake**

Test were performed with and without the air-handler intakes operating. When the vacuum system was operating, the smoke would largely be captured by the vent wells, while without the vacuums in operation, the smoke would spread over the surface.

**b) Vent Location**

As a result of the relative locations on the roof top of the wells, and the elevator building, flow separation often occurs which directs the smoke over the intakes. With the building features and vacuum intakes working in combination, the smoke can be seen to flow perpendicular and even opposite to the primary wind direction.

**c) Solid Fence**

Three different configurations of solid fences were tested. They tended to slow and lift the smoke as it approached and passed over the fence, but they did not significantly reduce the amount of smoke reaching the intake vents regardless of the fence configuration.

**d) Porous Fence**

Four fence configurations were tested by using a screen material with 50% porosity. Aside from slowing the air flow slightly, the porous fence did little to prevent the smoke from entering the intake vents.

**e) Canopy**

Canopies with varying heights and overhangs were tested. They seemed to deflect slightly more smoke as their height decreased, and their overhang increased. The height appeared to have considerably more influence than any other factors for preventing the smoke's entrance into the vent areas.

**f) Fence and Canopy Combinations**

A considerable amount of smoke was directed over the canopy roof as a result of the upwind fence, however the fence on the downwind side tended to re-direct the flow such that smoke passing across the canopy was drawn back down into the ventilation wells.

**g) Flat Roof Cover**

The flat roof appeared to have a similar effect to that of the canopy on the flow of the smoke. Smoke below the roof level of the cover was sucked down into the vents, and most smoke passing above the cover went downwind undisturbed.

**h) Flat roof Cover and Solid Fence Combination**

A fence one half the height of the flat roof cover was located around the intake wells, underneath the flat roof cover. This combination appeared to be quite effective in diverting most of the smoke away from the vents. Locating the fence under the cover and not simply around its perimeter seemed to provide a considerable advantage.

**i) Site Orientation: N, NE, E, SE**

The model was rotated to examine a variety of approach wind directions. As the flow interacted with the structure and shelter configurations, the smoke plume's trajectory was modified into various streamline patterns.

Several patterns reoccurred no matter which building configuration was examined. Winds from the NE and SE directions were split by the building's corners(and the elevator building), and were convected directly over the intake vents.

**j) Wind Speed**

While higher velocity winds did allow slightly more smoke to pass over the intake vents, they did not significantly mitigate smoke intake by the ventilation wells.

Conclusions from Smoke Visualization Tests:

The visualization tests provided observations which provided focus for the simulated snow experiments. The major conclusions were:

The solid and porous fences, without regard to location were ineffective in minimizing smoke inhalation by the two ventilation wells.

The canopy and flat roof covers appeared to significantly reduce the amount of smoke entering the wells. Other factors, such as reducing the distance from the top of the well to the bottom edge of the canopy (or cover), or the addition of a solid fence below the cover (or canopy) appeared to assist in diverting the smoke away from the intake wells.

## 3.2 Snowdrift Results

Table 5 lists all the snow simulation runs performed. A 1/2" VHS television tape was provided separately to the sponsor.

A total of 40 simulated snow test cases were performed to evaluate the effectiveness of various fence, canopy, and flat roof configurations. The tests were grouped by configuration in a progressive order of wind orientation.

Figure 27 and Figure 28 indicate the snow deposition rates for each configuration for two wind directions. Abbreviations for different shelter configurations are found in Table 5.

**a) Solid Fence**

Three different solid fence configurations were tested (A, B and C). The fences stopped snow close to the roof top, but had little effect on snow that was deflected over the fence. Drifts of snow accumulated in front of the solid fences, indicating that they could be used to control snow drifting problems on the building roof top.

**b) Porous Fence**

Four different porous fence configurations were tested (A, B, C and D). The porous fences were located further away from the vent intakes than were the solid fence. The porous fences stopped some snow in their immediate vicinity, but failed to have much effect upon the snow entering the ventilation wells. Configuration D was probably the most effective of the porous fences, perhaps due to its closer proximity to the smaller intake.

c) Canopy

Canopies of various heights and overhang were tested. This style of mitigation shelter proved to be quite effective. The amount of "snow" (borax) deposited in the intake wells was reduced by a factor of ten or more (refer to Figure 27 and Figure 28). As the height of the canopy was reduced, its effectiveness increased. Increasing height reduced the ability of the canopy to prevent the snow's entrance to the well.

d) Fence and Canopy Combination

The results from these tests were disappointing. The presence of the fence around the outer edge of the canopy appeared to redirect the vacuum from the intake in such a way that snow passing near or just over the canopies was forcefully sucked down into the vent. Placement of the fence further away had little measurable effect on the amount of snow collected in the intake vents.

e) Flat Roof Cover

The flat roof configuration was slightly more successful in preventing the entrainment of "snow" into the vents than the canopy. Its flat, rather than tilted roof allowed the air flow to carry the "snow" over the vent with less disturbance.

f) Flat Roof Cover and Solid Fence Combination

This style of mitigation measure was the most effective of the configurations tested. The shorter fence, just inside the perimeter of the flat cover added to the effectiveness of the cover in preventing snow from entering the intake vents.

g) Site Orientation N, NE

The model was tested in two primary wind directions for all the configurations. The same snow patterns were consistently observed on the roof top, with slight discrepancies being caused by the various mitigating measure being examined.

h) Wind Speed

Considerably higher velocity winds (about 4 m/s) were required to cause the deposited snow on the building's roof to move and form new snow drift patterns. When movement occurred, it did not result in much additional snow deposition in the intake wells.

i) Vacuum Intake

Tests were performed with and without the vacuum intakes operating. The general snow patterns were relatively unchanged by the presence or absence of the vacuum. But the amount of snow in the vent wells with the vacuums in operation larger than that without the vacuums in operation.

Conclusions from Simulated Snow Tests:

The fence configurations, both solid and porous, had very little impact upon the amount of snow which accumulated in the intake wells. Their measurable impact decreased as their proximity to the vents decreased.

Both the canopy and flat roof cover proved to be consistently very effective in preventing large amounts of snow from entering the intake wells. Factors such as decreased height also improved their performance.

A fence inside the perimeter of the cover added to its effectiveness in preventing the simulated snow's entrance to the vent.

## 3.3 Recommendation

Based on the configurations examined during this study a flat topped canopy should be constructed over each air-handler well on the UCHSC roof-top. the canopy should have eaves which overhang the edges of the well by a distance approximately equal to their height above the roof. Snow entrainment can be further reduced by placing a barrier wall under the edge of the canopy. This barrier should rise about half the height of the canopy itself, and it should be placed half way between the edge of the well and the roof overhang.

## REFERENCES

Allwine, D.J., Meroney, R.N. and Peterka, J.A. (1979), "Rancho Seco Building Wake Effects on Atmospheric Diffusion: Simulation in a Meteorological Wind Tunnel," Technical Report for U.S. Nuclear Regulatory Commission.

Anno, Y. (1984), "Requirements for Modeling of a Snowdrift," Cold Reg. Sci. Technol., 8(3):241-252.

Anno, Y. (1985), "Supplement to Anno's Modeling Conditions for a Snowdrift," Cold Reg. Sci. Technol., 10(1985) 193-195.

Anno, Y. (1989), "Froude Number Paradoxes in Modeling of Snowdrift," Sixth U.S. National Conference on Wind Engineering, Houston, Texas, Vol.II, A6-(44-46).

Becker, A. (1944), "Natural Snow Fences Along Roads," Bautechnik, 22, 37-42.

Briggs, G.A. (1986), "Research on Diffusion in Atmospheric Boundary Layers: A Position Paper on Status and Needs," Atmospheric Sciences Research Laboratory, U.S. E.P.A., Research Triangle Park, North Carolina, 227 pp.

Davies, M.E. and Inman, P.N. (1986), "Wind Tunnel Modelling of the Thorney Island Heavy Gas Dispersion Trials," Gas Research Institute Contract No. 5084-252-1016, British Maritime Technology, U.K.

Finney, E. A. (1937), "Snow Control by Tree Planting, Part VI, Wind Tunnel Experiments on Tree Plantings," Michigan Engineering Bulletin No. 75, Michigan Engineering Experiment Station.

Gray, D.M. and Male, D.H., editors (1981), "Handbook of Snow: Principles, Processes, Management and Use," Pergamon Press, New York.

Hatcher, R.V., Meroney, R.N., Peterka, J.A. and Kothari, K. (1977), "Dispersion in the Wake of a Model Industrial Complex," Technical Report for U.S. Nuclear Regulatory Commission.

Huber, A. (1981), "Guideline for Use of Fluid Modeling to Determine Good Engineering Practice Stack Height", EPA-450/4-81-003, USEPA.

Iversen, J. D. (1979a), "Drifting Snow Similitude," J. Hydraulics Division, Proceedings of the American Society of Civil Engineers, 105, HY6, 737-753.

Iversen, J. D. (1979b), "Drifting Snow Similitude - Drift Deposit Rate correlation," Fifth International Conference on Wind Engineering, Ft. Collins, Colorado, Proceedings, Paper VIII-6, 1.

Iverson, J.D. (1980a), "Wind-Tunnel Modeling of Snow Fences and Natural Snow-Drift Controls," Proceedings of 37th Eastern Snow Conference, Peterborough, Ontario, Canada, pp. 106-124.

Iverson, J.D. (1980b), "Drifting-Snow Similitude - Transport-Rate and Roughness Modeling," J. Glaciol., 26, pp. 393-403.

Iverson, J.D. (1981), "Comparison of Wind-Tunnel Model and Full-Scale Snow Fence Drifts," J. of Wind Engr. and Ind. Aerody., 8, pp.231-249.

Iversen, J. D. (1989), "The Effect of a Roughness Element on Local Saltation Transport," Sixth U.S. National Conference on Wind Engineering, Houston, Texas. Vol.II, A6-(1-10).

Kind, R. J. (1976), "A Critical Examination of the Requirements for Model Simulation of Wind-Induced Erosion/Deposition Phenomena Such as Snow Drifting," Atmos. Environ., 10, 219-227.

Kothari, K. and Meroney, R.N. and Peterka, J.A. (1979), "Nuclear Power Plant Building Wake Effects on Atmospheric Diffusion: Simulation in Wind Tunnel," Technical Report for Electric Power Research Institute, EPRI NP-1891.

Meroney, R.N., Bowen, A.J., Lindley, D. and Pearse, J.R. (1978), "Wind Characteristics over Complex Terrain: Laboratory Simulation and Field Measurements at Rakaia Gorge", New Zealand, U.S. Dept. of Energy Report RLO/2438-77/2, 219 pp.

Meroney, R.N. (1980), "Physical Simulation of Dispersion in Complex Terrain and Valley Drainage Flow Situations", Proceedings 11th NATO/CCMS International Technical Meeting on Air Pollution Modeling and Its Applications, Amsterdam, the Netherlands, 25-28 November 1980, 21 pp.

Meroney, R.N. (1982), "Building Aerodynamics", Chapter 11 from Engineering Meteorology, (ed. E.Plate), Elsevier Publishing Company, New York.

Meroney, R.N. and Meroney, B.N. (1988), "Snow Control with Vortex and Blower Fences," Proceedings of Conference on A Multidisciplinary Approach to Snow Engineering, 10-15 July 1988, Santa Barbara, California, 11 pp.

Nokkentved, C. (1940), "Drift Formation at Snow Fences," Stads-og Haveingenoren, 31, #9.

Odar, F. (1962), "Scale Factors for Simulation of Drifting Snow," J. Engineering Mechanics Division, ASCE, 88, EM2, 1-16.

Odar, F. (1965), "Simulation of Drifting Snow," Research Report 174, cold Regions Research and Engineering Laboratory, Hanover, new Hampshire.

Snyder, W.H. (1981), "Guidelines for Fluid Modeling of Atmospheric Diffusion", EPA Report EPA-600/8-81-009, USEPA, 185 pp.

Sutton, O.G. (1953), "Micrometeorology", McGraw-Hill Book Company, Inc.

Tabler, R.D. (1981a), "Geometry and Density of Drifts Formed by Snow Fences," J. Glaciol., 26, No. 94.

Tabler, R.D. (1981b), "Self-similarity of wind profiles in blowing snow allows outdoor modelling," J. Glaciol., 26, No. 94.

Woodruff, N.A. and Zingg, A.W. (1952), "Wind-Tunnel Studies of Fundamental Problems Related to Windbreaks," U.S. Dept. of Agriculture, Soil Conservation Service, SCS-TP-112.

# TABLES

**Table 1** Hot-Wire Calibration Data

HOT WIRE CALIBRATION DATA FROM "WRCAL"

| | | | |
|---|---|---|---|
| DATE | = 06-08-89 | TIME | = 15:06:48 |
| PRESSURE (mmHg) | = 630. | TEMPERATURE (C) | = 23.0 |
| MIN. VELOCITY | = 25.3 | MAX. VELOCITY | = 288. |
| # WIRES | = 1 | # POINTS | = 10 |
| VELOCITY UNITS | = cm/s | | |

| ACTUAL VEL. | VOLTAGES OUT | ERROR (%) | CALCU VEL. |
|---|---|---|---|
| 25.30 | 2.552 | -0.3 | 25.21 |
| 50.59 | 2.714 | 0.2 | 50.69 |
| 74.18 | 2.821 | 0.2 | 74.36 |
| 97.13 | 2.905 | 0.0 | 97.14 |
| 123.1 | 2.986 | 0.0 | 123.13 |
| 143.4 | 3.042 | 0.0 | 143.43 |
| 173.1 | 3.115 | 0.1 | 173.25 |
| 216.4 | 3.205 | -0.4 | 215.48 |
| 241.9 | 3.255 | 0.0 | 241.95 |
| 288.3 | 3.336 | 0.2 | 288.86 |

A = 4.2230
B = 0.5312
C = 0.4526

**Table 2** Velocity Profile Data for 1:50 Scale Model

Type profile 0>volt, 1>wire, 2>x-wire, 4>pito = 1
Number of profiles in the file = 1
Number of points per profile = 18
Units of Height = cm
Units of Velocity = cm/s
Units of Turbulence Intensity = %
Units of Temperature = °C

| Height | Velocity | RMS | Tur. Int. | Temp. |
|---|---|---|---|---|
| 1.50 | 169.76 | 38.34 | 22.58 | 23.00 |
| 2.33 | 176.29 | 39.99 | 22.69 | 23.00 |
| 3.35 | 183.26 | 44.02 | 24.02 | 23.00 |
| 4.01 | 190.24 | 39.91 | 20.98 | 23.00 |
| 5.95 | 216.56 | 38.44 | 17.75 | 23.00 |
| 7.97 | 223.70 | 38.08 | 17.02 | 23.00 |
| 11.91 | 243.00 | 34.59 | 14.23 | 23.00 |
| 16.11 | 245.03 | 35.18 | 14.36 | 23.00 |
| 20.14 | 238.64 | 33.90 | 14.20 | 23.00 |
| 29.81 | 240.61 | 32.80 | 13.63 | 23.00 |
| 39.87 | 238.58 | 36.34 | 15.23 | 23.00 |
| 50.19 | 246.66 | 36.54 | 14.82 | 23.00 |
| 60.18 | 257.03 | 36.62 | 14.25 | 23.00 |
| 69.77 | 254.67 | 33.88 | 13.30 | 23.00 |
| 79.83 | 255.40 | 34.47 | 13.49 | 23.00 |
| 89.93 | 259.41 | 33.94 | 13.08 | 23.00 |
| 100.03 | 266.79 | 35.23 | 13.20 | 23.00 |
| 120.06 | 273.67 | 35.95 | 13.14 | 23.00 |

Table 3 Field and Model Flow Rates for the Intake Areas on the Roof

| Intake # | Qp (cfm*1000) | Area W*H (ft) | Qm (cfm) |
|---|---|---|---|
| SF-3 | 64 | 20*11.42 | 25.6 |
| SF-5 | 30 | 11.92*11.5 | 12.0 |
| SF-8 | 56.3 | 20*11.42 | 22.5 |
| SF-9 | 104 | 22*11.5 | 41.6 |
| SF-10 | 104 | 22*11.5 | 41.6 |
| SF-11 | 34.7 | 11.92*11.5 | 13.9 |

The small intake area on the roof is the combination of SF-3 & SF-8.
The big intake area is the combination of SF-5, SF-9, SF-10 & SF-11.

| Intake Area | Qm (cfm) | Area (in*in) | Speed (ft/s) |
|---|---|---|---|
| Big | 109.1 | 5.51*7.48 | 6.36 |
| Small | 48.1 | 2.76*4.72 | 8.86 |

Table 4 Visualization Test Data

| Run # | Config. | WD | Speed | Index |
|---|---|---|---|---|
| 1 | None | N | 1 m/s | 130 |
| 2 | None | NE | 1 m/s | 267 |
| 3 | None | E | 1 m/s | 410 |
| 4 | None | SE | 1 m/s | 538 |
| 5 | None | N | 2 m/s | 688 |
| 6 | None | NE | 2 m/s | 806 |
| 7 | None | E | 2 m/s | 942 |
| 8 | None | SE | 2 m/s | 1067 |
| 9 | None | N | 3 m/s | 1193 |
| 10 | None | NE | 3 m/s | 1317 |
| 11 | None | E | 3 m/s | 1454 |
| 12 | None | SE | 3 m/s | 1553 |
| 13 | Solid A | N | 3 m/s | 1673 |
| 14 | Solid A | NE | 3 m/s | 1774 |
| 15 | Solid A | E | 3 m/s | 1875 |
| 16 | Solid A | SE | 3 m/s | 1968 |
| 17 | Solid A | N | 1 m/s | 2063 |
| 18 | Solid A | NE | 1 m/s | 2165 |
| 19 | Solid A | E | 1 m/s | 2260 |
| 20 | Solid A | SE | 1 m/s | 2353 |
| 21 | Solid B | N | 1 m/s | 2445 |
| 22 | Solid B | NE | 1 m/s | 2523 |
| 23 | Solid B | E | 1 m/s | 2601 |
| 24 | Solid B | SE | 1 m/s | 2686 |
| 25 | Solid C | N | 1 m/s | 2772 |
| 26 | Solid C | NE | 1 m/s | 2854 |
| 27 | Solid C | E | 1 m/s | 2942 |
| 28 | Solid C | SE | 1 m/s | 3022 |
| 29 | Fence A | N | 1 m/s | 3119 |
| 30 | Fence A | NE | 1 m/s | 3189 |
| 31 | Fence A | E | 1 m/s | 3277 |
| 32 | Fence A | SE | 1 m/s | 3344 |
| 33 | Fence B | N | 1 m/s | 3441 |
| 34 | Fence B | NE | 1 m/s | 3503 |
| 35 | Fence B | E | 1 m/s | 3563 |
| 36 | Fence B | SE | 1 m/s | 3635 |
| 37 | Fence C | N | 1 m/s | 3708 |
| 38 | Fence C | NE | 1 m/s | 3746 |
| 39 | Fence C | E | 1 m/s | 3798 |
| 40 | Fence C | SE | 1 m/s | 3844 |
| 41 | Fence D | N | 1 m/s | 3913 |
| 42 | Fence D | NE | 1 m/s | 3960 |
| 43 | Fence D | E | 1 m/s | 4016 |
| 44 | Fence D | SE | 1 m/s | 4085 |
| 45 | Canopy A | N | 1 m/s | 4136 |
| 46 | Canopy A | NE | 1 m/s | 4173 |
| 47 | Canopy A | E | 1 m/s | 4209 |
| 48 | Canopy A | SE | 1 m/s | 4229 |
| 49 | Canopy C | N | 1 m/s | 4266 |
| 50 | Canopy C | NE | 1 m/s | 4295 |
| 51 | Canopy C | E | 1 m/s | 4341 |
| 52 | Canopy C | SE | 1 m/s | 4366 |
| 53 | Combin A | N | 1 m/s | 4385 |
| 54 | Combin A | NE | 1 m/s | 4440 |
| 55 | Combin B | N | 1 m/s | 4491 |
| 56 | Combin B | NE | 1 m/s | 4536 |
| 57 | Canopy D | N | 1 m/s | 4589 |
| 58 | Canopy D | NE | 1 m/s | 4635 |
| 59 | Canopy E | N | 1 m/s | 4697 |
| 60 | Canopy E | NE | 1 m/s | 4753 |
| 61 | None(NV) | N | 1 m/s | 4816 |
| 62 | None(NV) | NE | 1 m/s | 4867 |
| 63 | None(NV) | E | 1 m/s | 4921 |
| 64 | None(NV) | SE | 1 m/s | 4971 |
| 65 | Flat A | N | 1 m/s | 5023 |
| 66 | Flat A | NE | 1 m/s | 5071 |
| 67 | Flat B | N | 1 m/s | 5124 |
| 68 | Flat B | NE | 1 m/s | 5169 |

Comments: NV indicates no vacuum operating.

Table 5 Snowdrift Test Data

| Run # | Config. | Abbrv. | WD | Speed | Lg. Area (gram) | Sm. Area (gram) | Index |
|---|---|---|---|---|---|---|---|
| 1 | None | N | N | 1 m/s | 24 | 11 | 92 |
| 2 | None | N | NE | 1 m/s | 14.75 | 6.25 | 285 |
| 3 | None | N | E | 1 m/s | 30.5 | 4.5 | 467 |
| 4 | None | N | N | 3 m/s | 0 | 0 | 640 |
| 5 | Solid A | SA | N | 1 m/s | 37.75 | 8 | 827 |
| 6 | Solid A | SA | NE | 1 m/s | 29.75 | 6 | 981 |
| 7 | Solid B | SB | N | 1 m/s | 28 | 7 | 1137 |
| 8 | Solid B | SB | NE | 1 m/s | 3.5 | 1.8 | 1276 |
| 9 | Solid C | SC | N | 1 m/s | 26.5 | 3.5 | 1411 |
| 10 | Solid C | SC | NE | 1 m/s | 23.8 | 3 | 1543 |
| 11 | Fence A | FA | N | 1 m/s | 26.5 | 5 | 1670 |
| 12 | Fence A | FA | NE | 1 m/s | 24 | 4.2 | 1794 |
| 13 | Fence B | FB | N | 1 m/s | 26.5 | 7.5 | 1917 |
| 14 | Fence B | FB | NE | 1 m/s | 20.5 | 3 | 2033 |
| 15 | Fence C | FC | N | 1 m/s | 24 | 6 | 2150 |
| 16 | Fence C | FC | NE | 1 m/s | 14 | 2.75 | 2261 |
| 17 | Fence D | FD | N | 1 m/s | 24.8 | 5 | 2369 |
| 18 | Fence D | FD | NE | 1 m/s | 23.5 | 3.4 | 2476 |
| 19 | Canopy A | CA | N | 1 m/s | 0.75 | 3.75 | 2580 |
| 20 | Canopy A | CA | NE | 1 m/s | 1.3 | 1.6 | 2685 |
| 21 | Canopy B | CB | N | 1 m/s | 0.5 | 3.3 | 2787 |
| 22 | Canopy B | CB | NE | 1 m/s | 2.8 | 1.5 | 2886 |
| 23 | Canopy C | CC | N | 1 m/s | 1.3 | 4 | 2983 |
| 24 | Canopy C | CC | NE | 1 m/s | 3.3 | 1.3 | 3080 |
| 25 | Combin A | CBA | N | 1 m/s | 1.5 | 1.5 | 3176 |
| 26 | Combin A | CBA | NE | 1 m/s | 1 | 3.5 | 3272 |
| 27 | Combin B | CBB | N | 1 m/s | 1 | 2.8 | 3365 |
| 28 | Combin B | CBB | NE | 1 m/s | 0.75 | 7 | 3458 |
| 29 | None(S) | NS | N | 1-3 m/s | 0 | 0 | 3548 |
| 30 | None(I) | NI | N | 1-3 m/s | ---- | ---- | 3937 |
| 31 | None(NV) | NV | N | 1-4 m/s | 19.5 | 7.8 | 4183 |
| 32 | None(NV) | NV | NE | 1-4 m/s | 5 | 9 | 4486 |
| 33 | Canopy D | CD | N | 1 m/s | 4.2 | 0 | 4798 |
| 34 | Canopy D | CD | NE | 1 m/s | 7.75 | 0 | 4872 |
| 35 | Canopy E | CE | N | 1 m/s | 16.8 | 1 | 4946 |
| 36 | Canopy E | CE | NE | 1 m/s | 5 | 1 | 5018 |
| 37 | Flat A | FTA | N | 1 m/s | 2.5 | 0.5 | 5218 |
| 38 | Flat A | FTA | NE | 1 m/s | 2.5 | 0.6 | 5286 |
| 39 | Flat B | FTB | N | 1 m/s | 1 | 0.4 | 5357 |
| 40 | Flat B | FTB | NE | 1 m/s | 1 | 0.6 | 5416 |

Comments: "S" indicates that the snow was sprayed on the top.
"I" indicates that the snow was dropped at 1 m/s then increasing the speed to 3 m/s.
"NV" indicates no vacuum operating.

# FIGURES

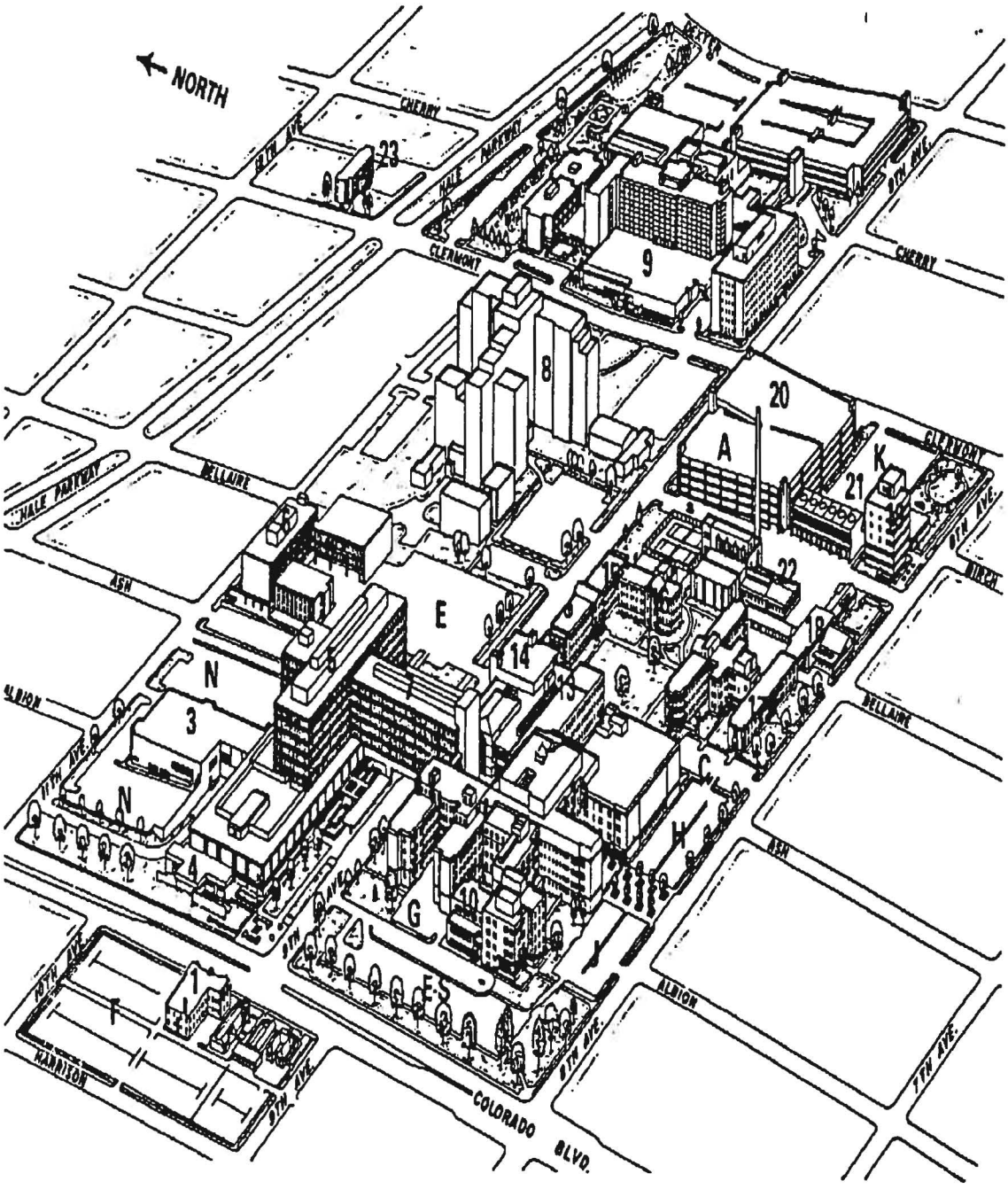


**Figure 1** Top View of the CU Denver Medical Health Center and Surrounding Buildings

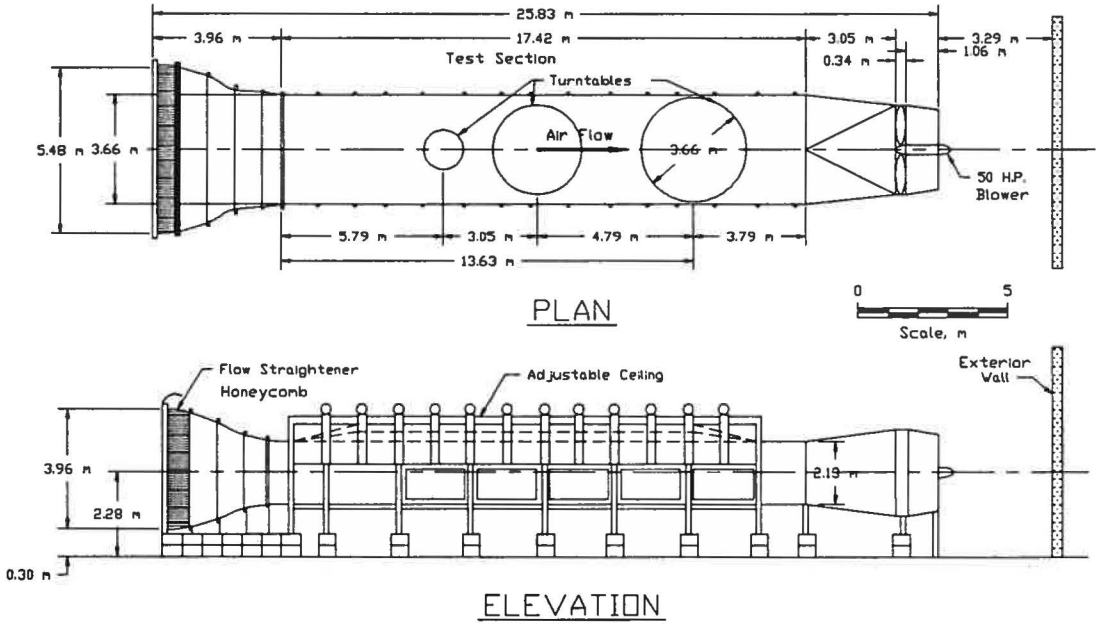


**Figure 2 Environmental Wind Tunnel**

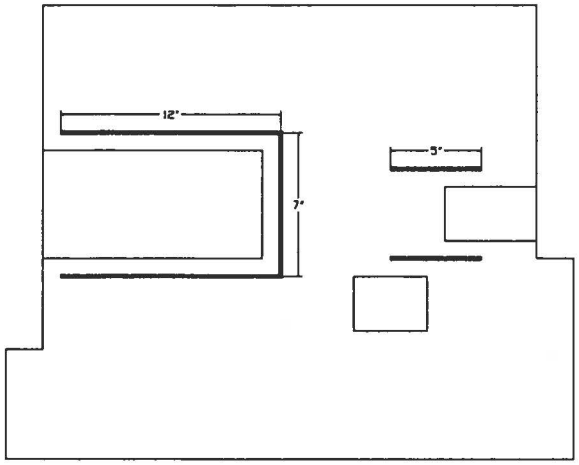


**Figure 3** Solid Barrier A

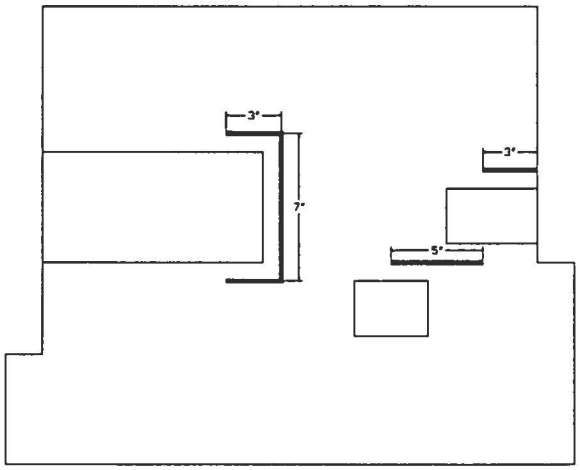


**Figure 4** Solid Barrier B

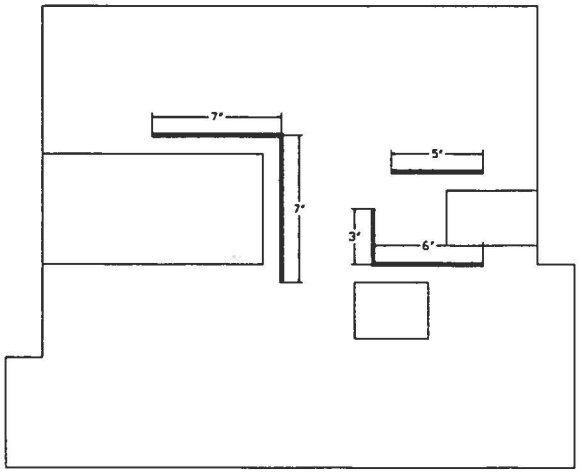


**Figure 5** Solid Barrier C

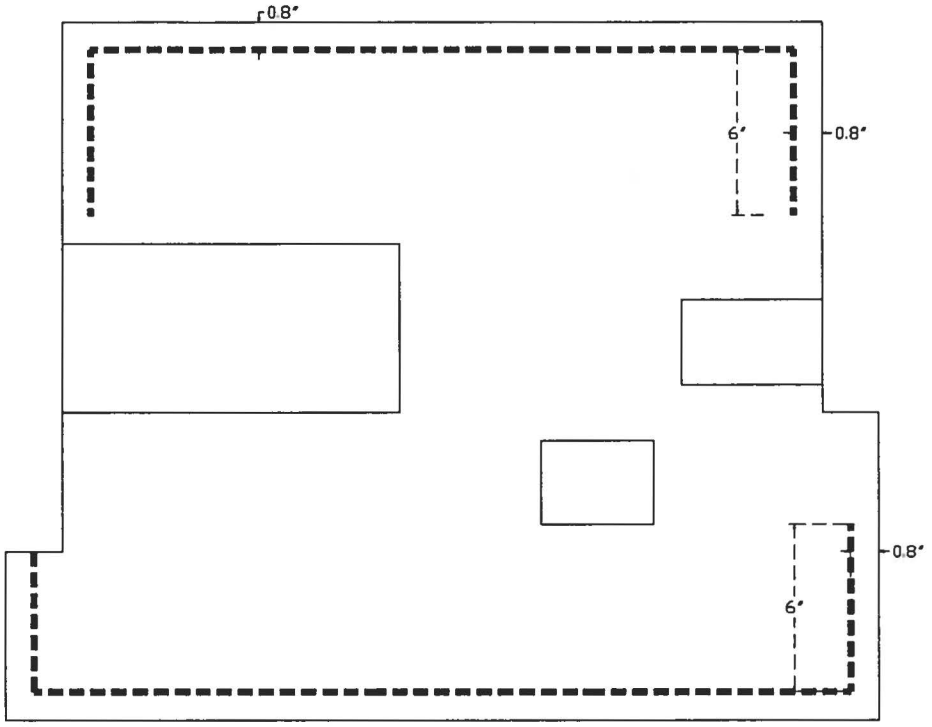


**Figure 6 Fence Configuration A**

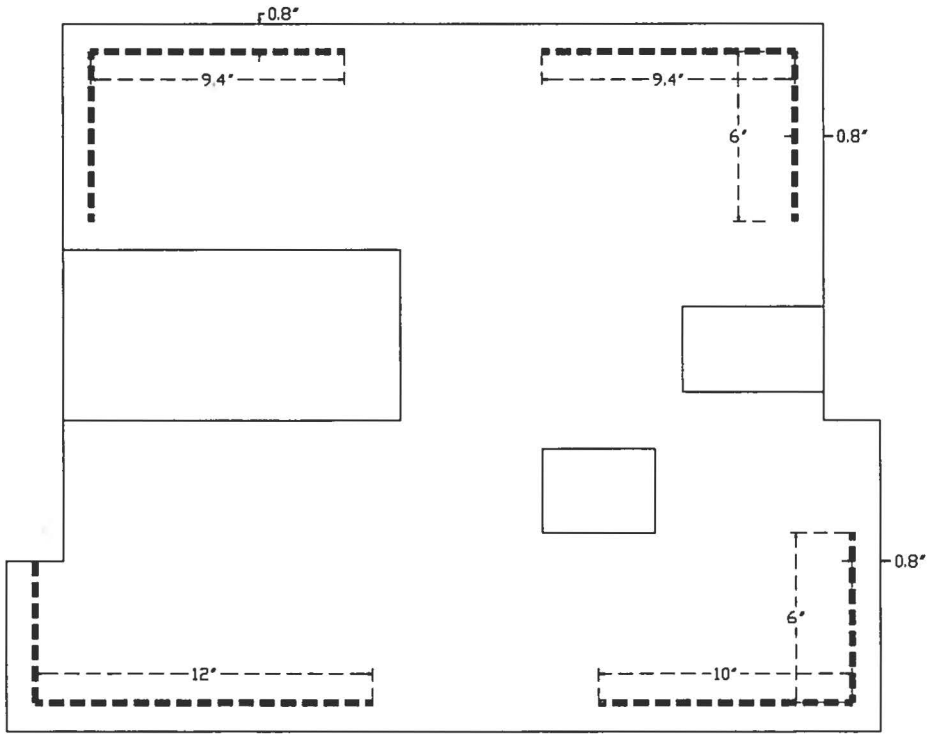


**Figure 7 Fence Configuration B**

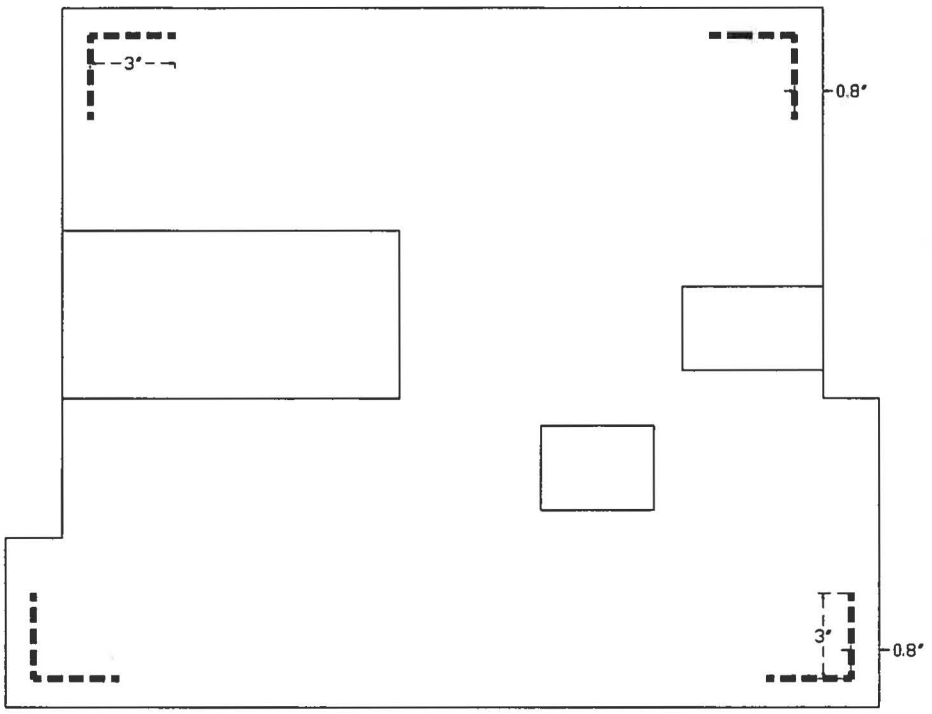


**Figure 8 Fence Configuration C**

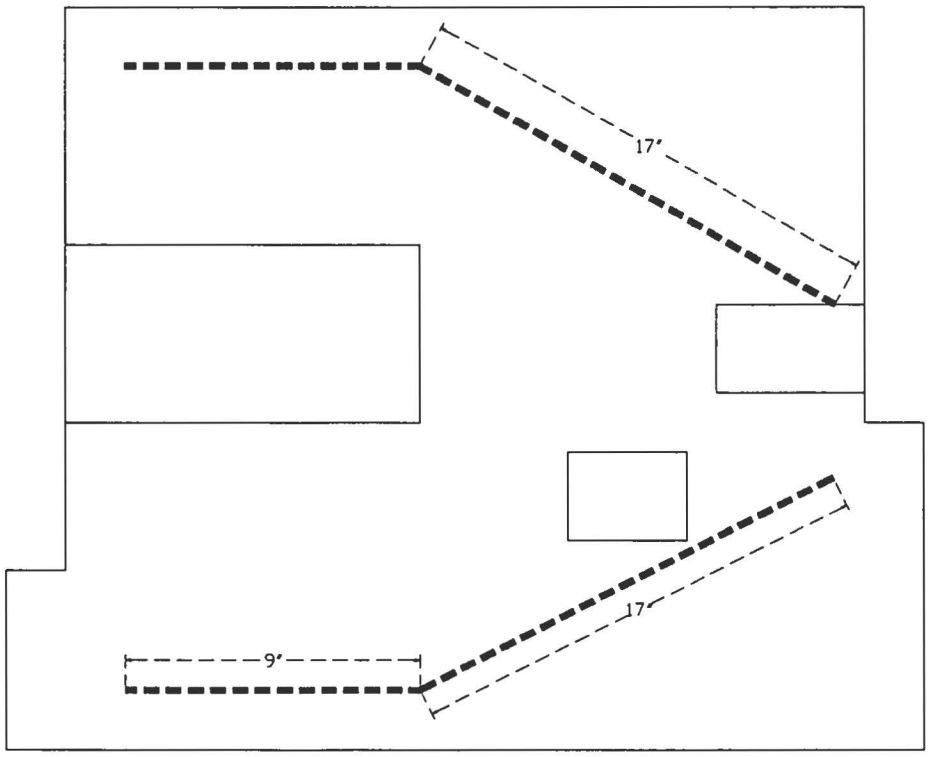


**Figure 9 Fence Configuration D**

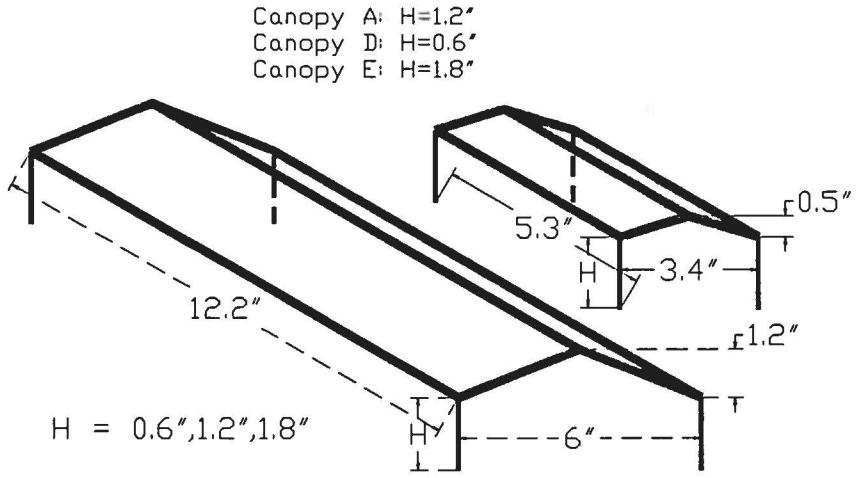


**Figure 10 Canopy A, D & E**

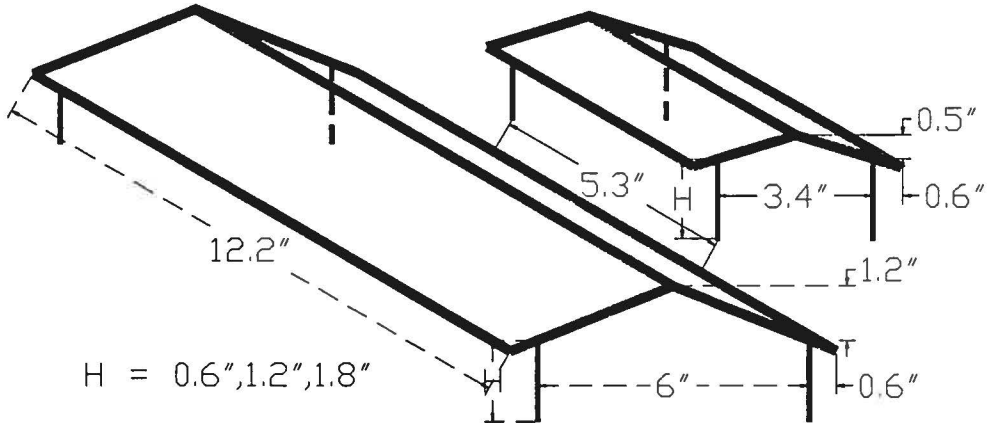


**Figure 11 Canopy B**

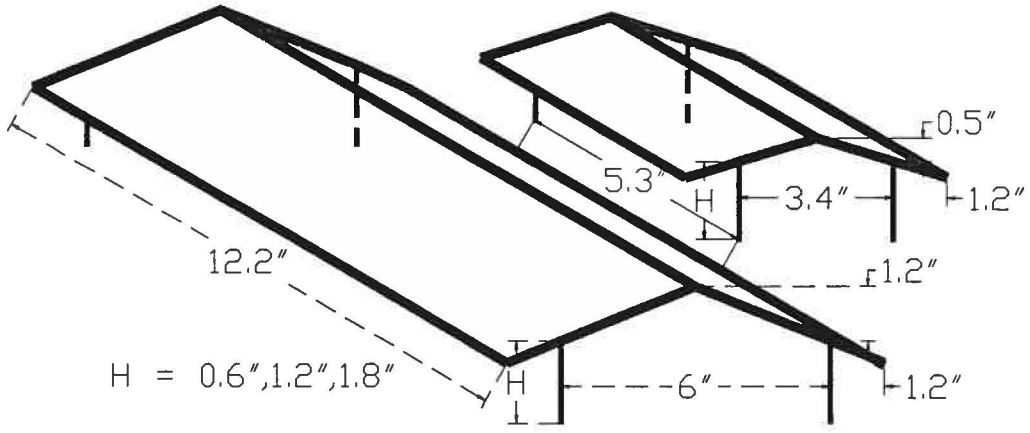


**Figure 12 Canopy C**

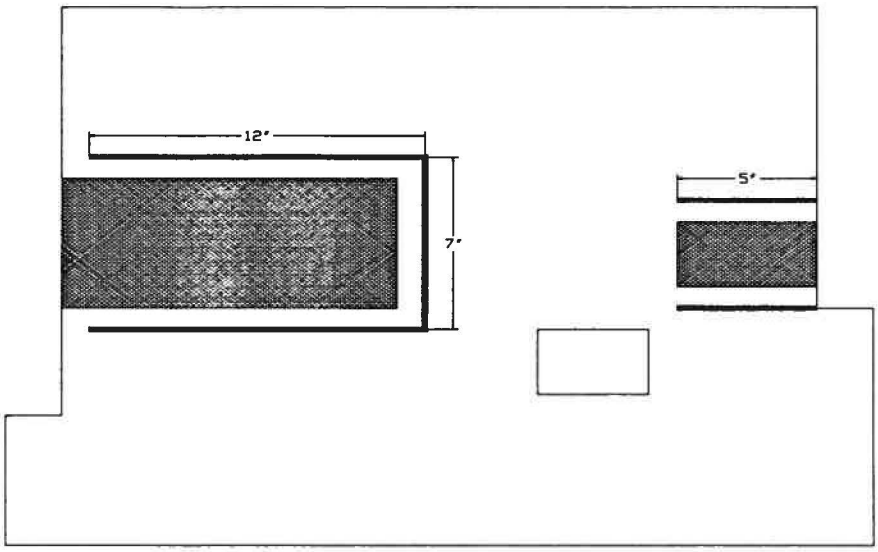


**Figure 13 Combine A**

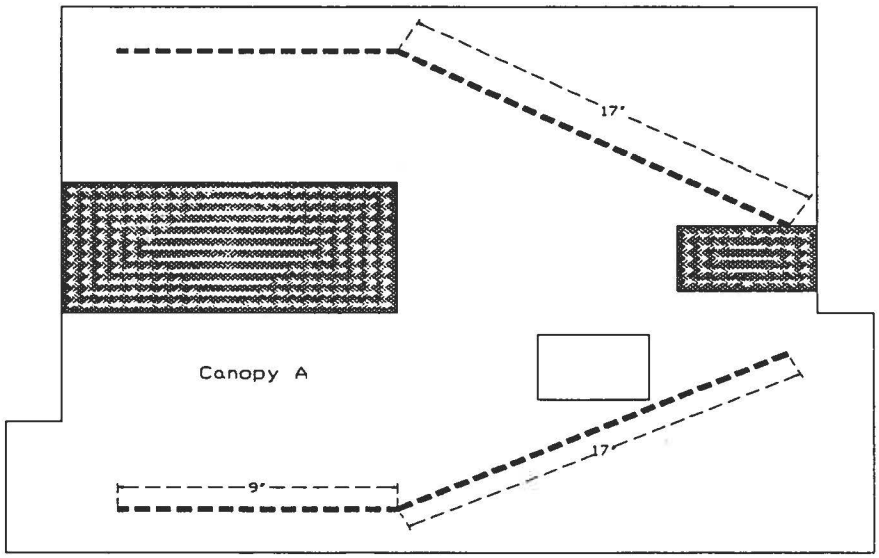


**Figure 14 Combine B**

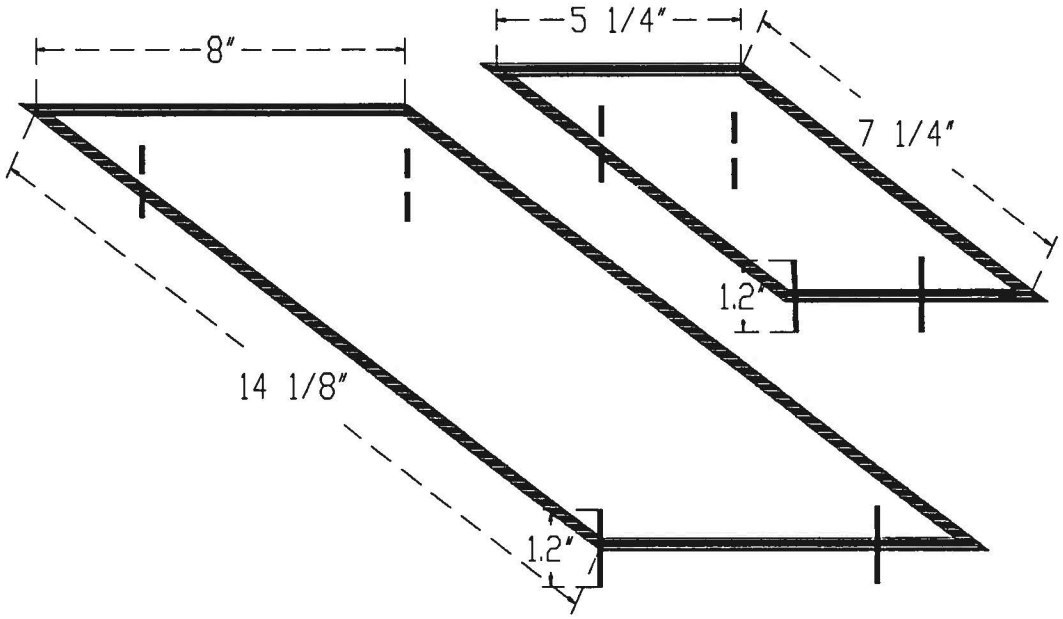


**Figure 15 Flat A**

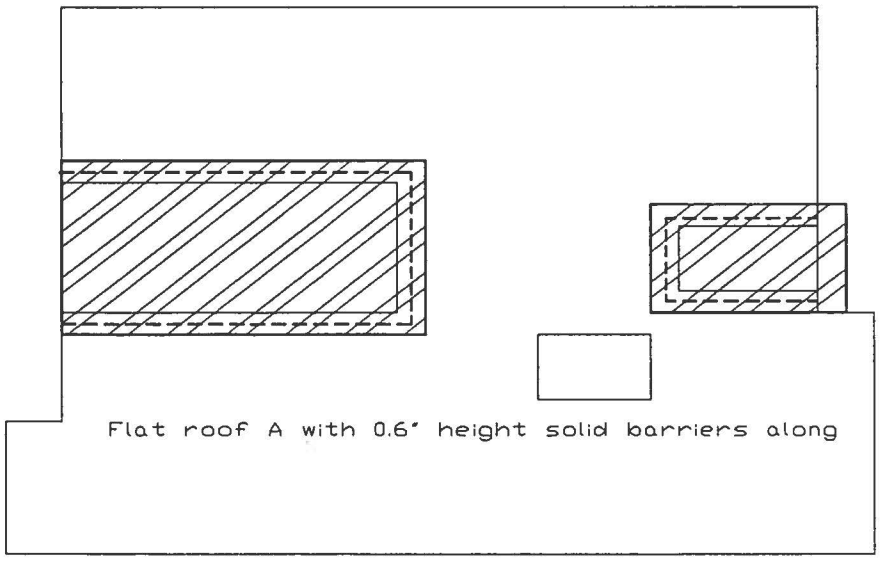


**Figure 16 Flat B**

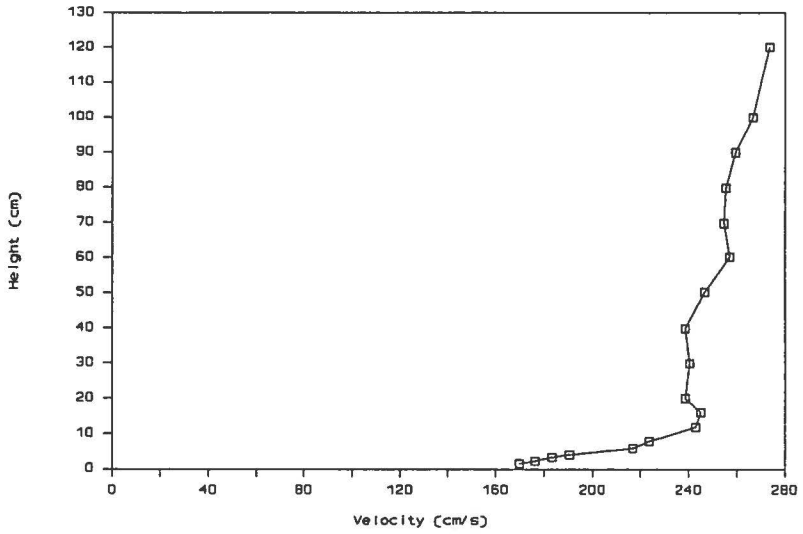


**Figure 17** Velocity Profile for 1:50 Scale Model

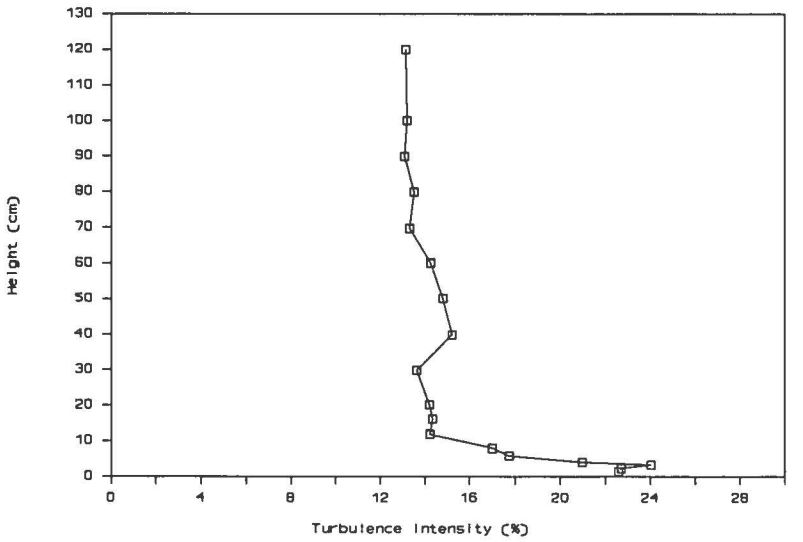


**Figure 18** Turbulence Profile for 1:50 Scale Model

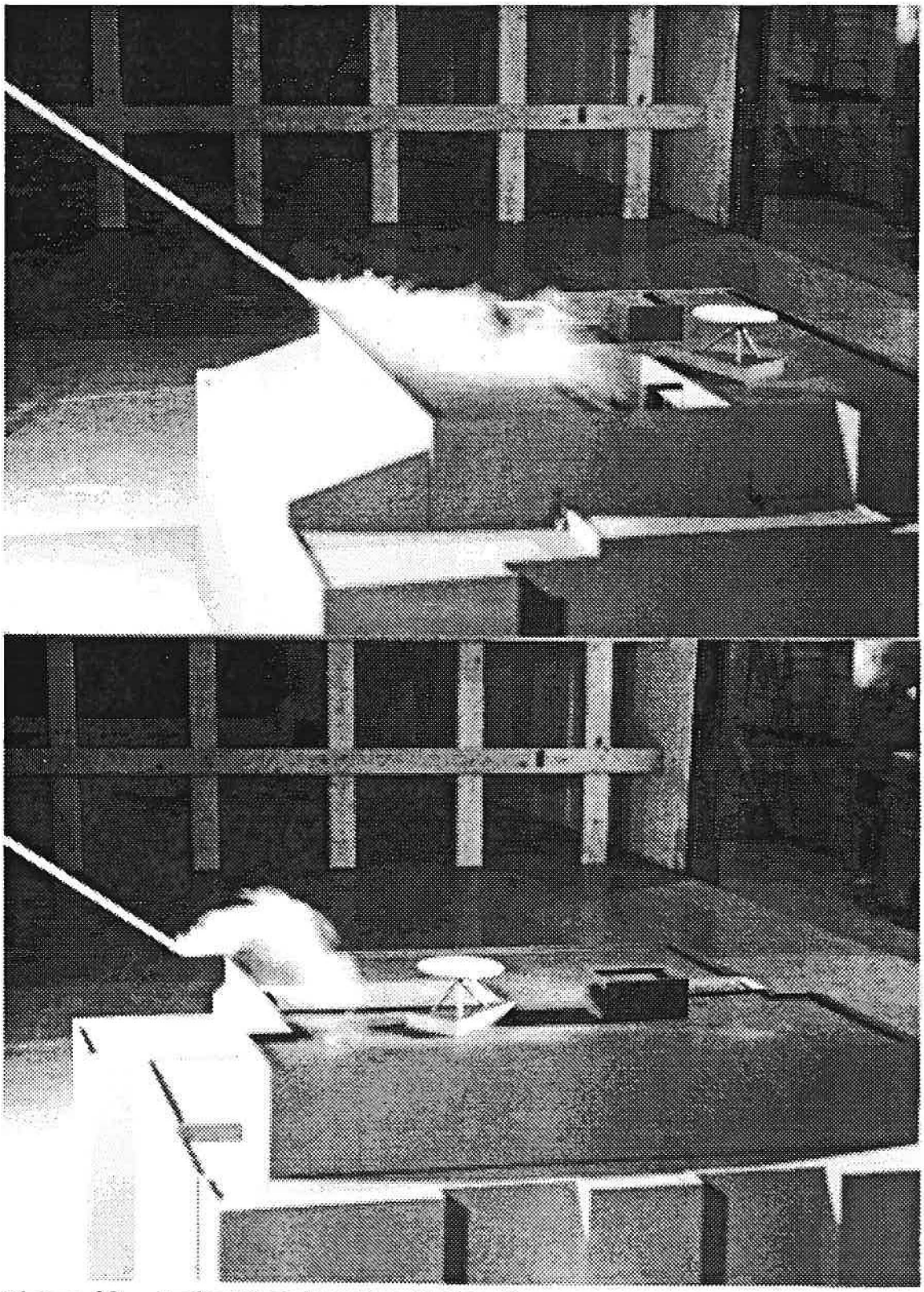

**Figure 19** Smoke Visualization Tests, I

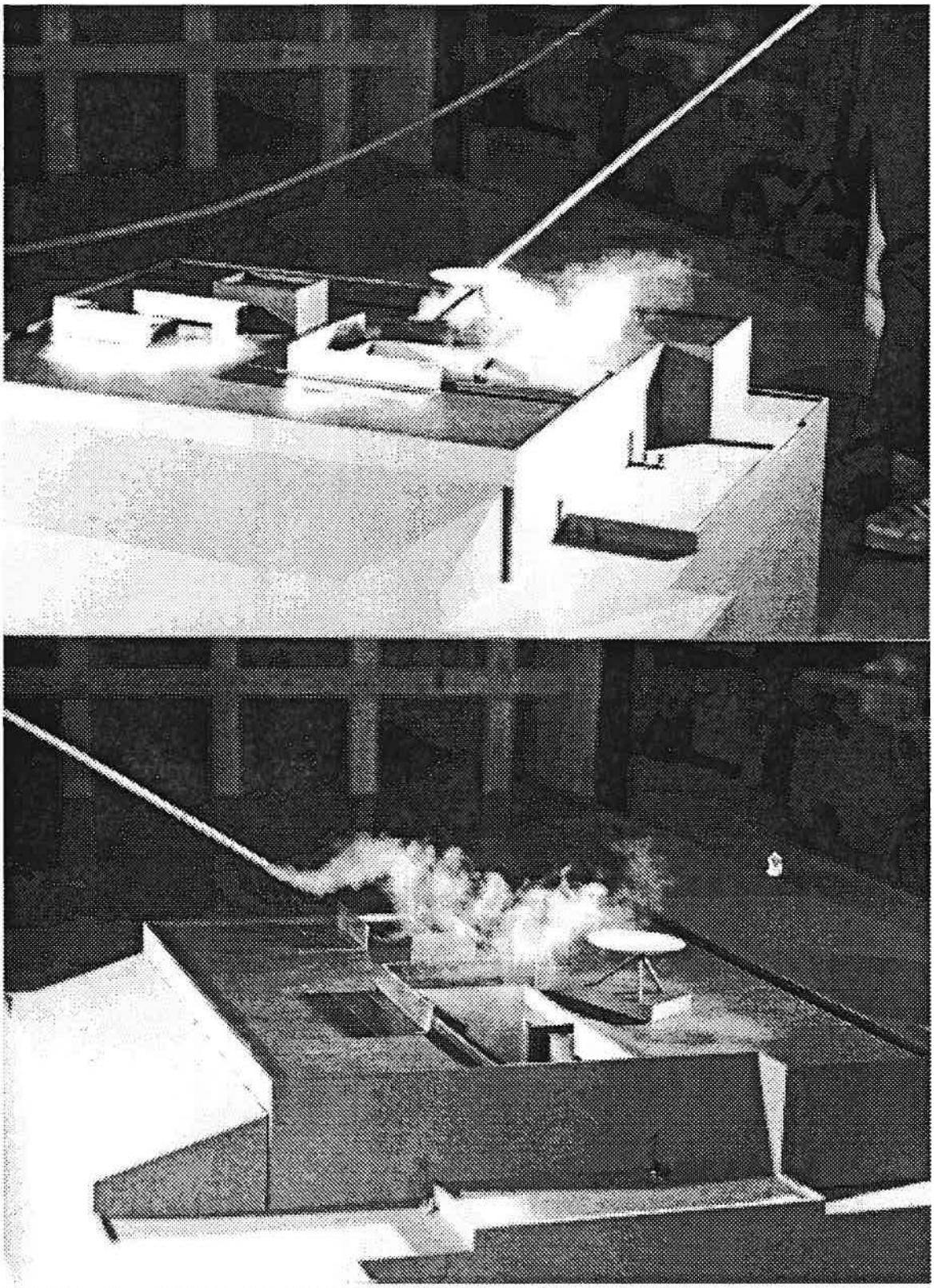

**Figure 20** Smoke Visualization Tests, II

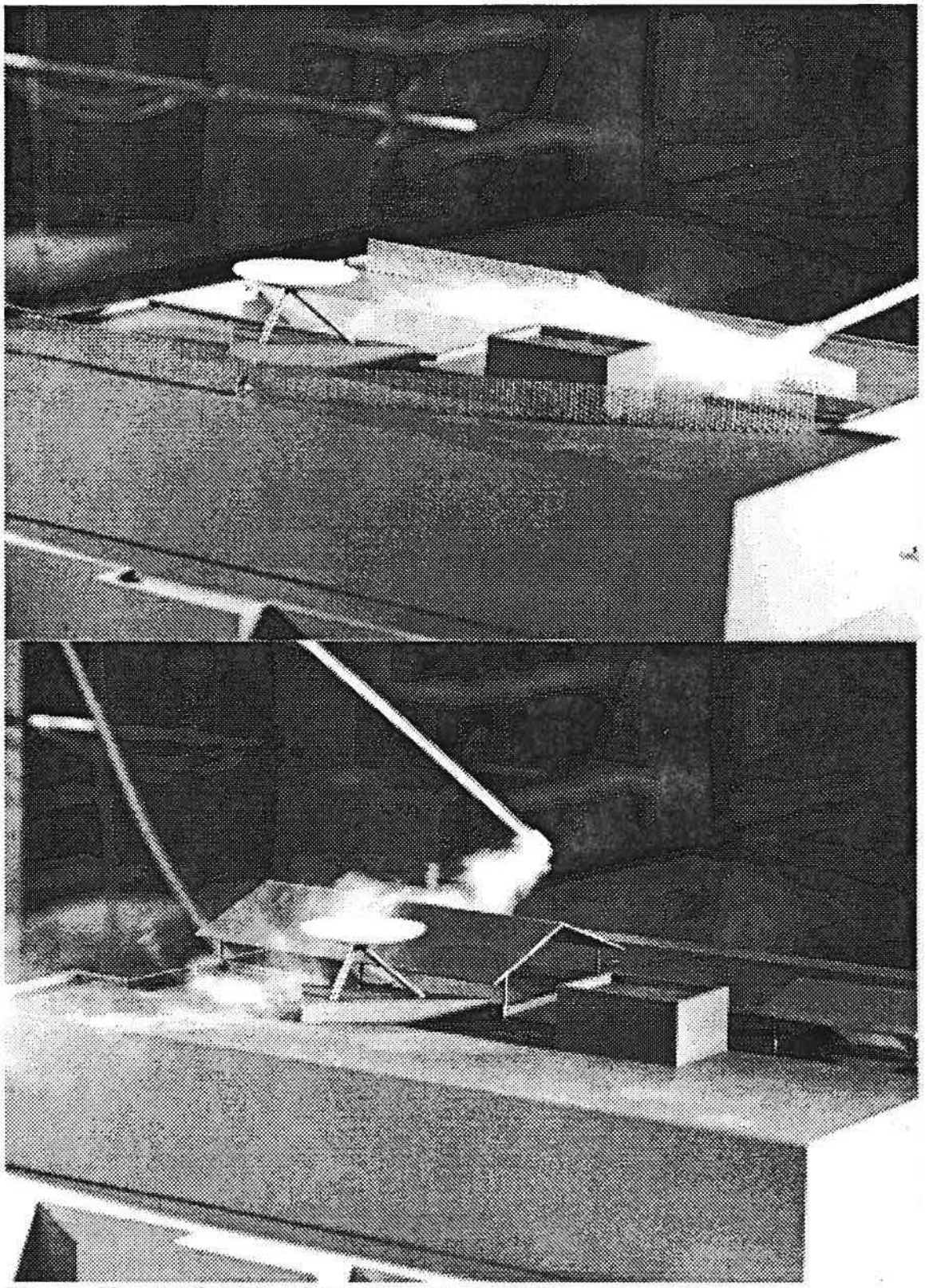

**Figure 21** Smoke Visualization Tests, III

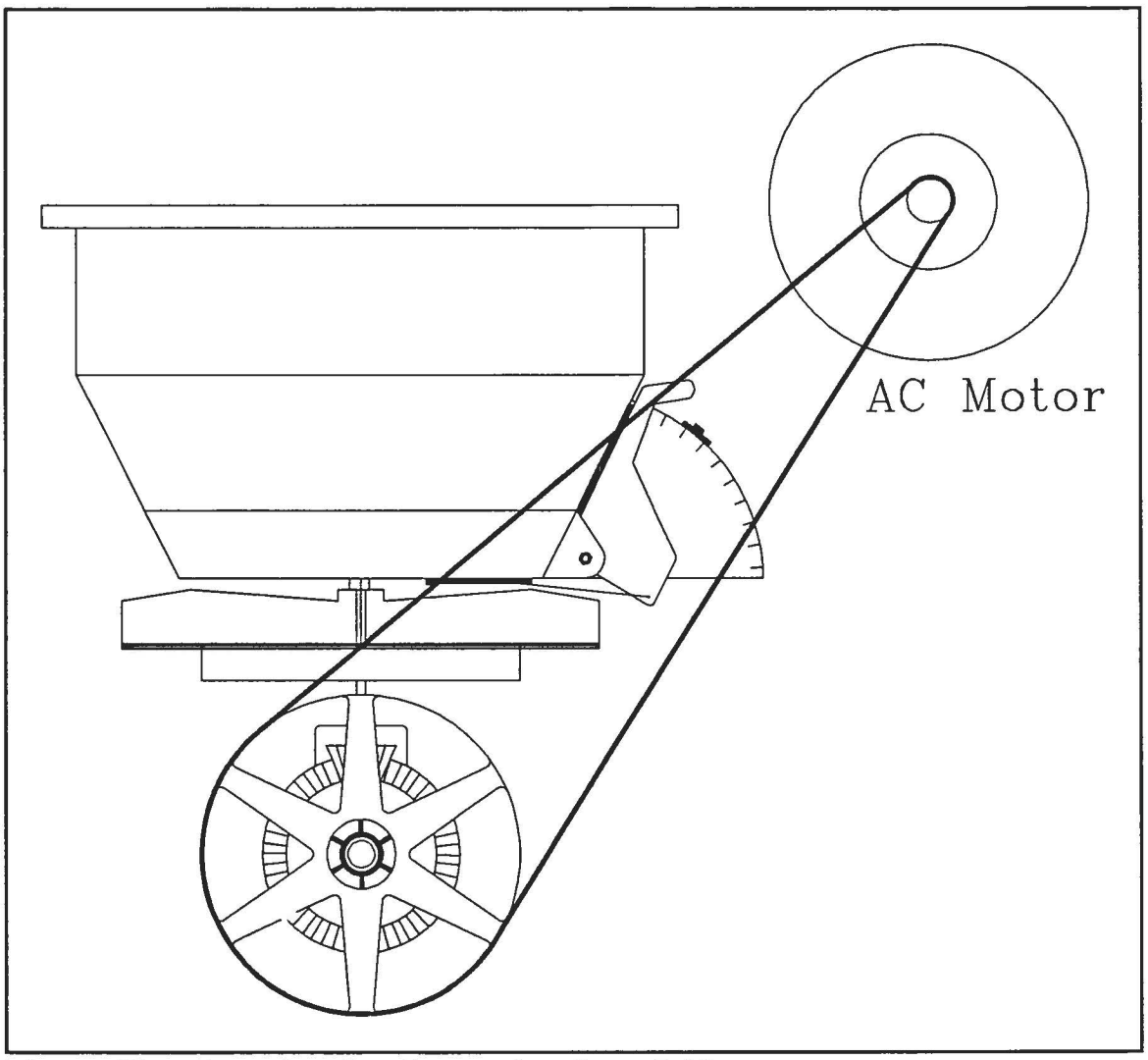


**Figure 22** Spreader for Generating Snow Fall

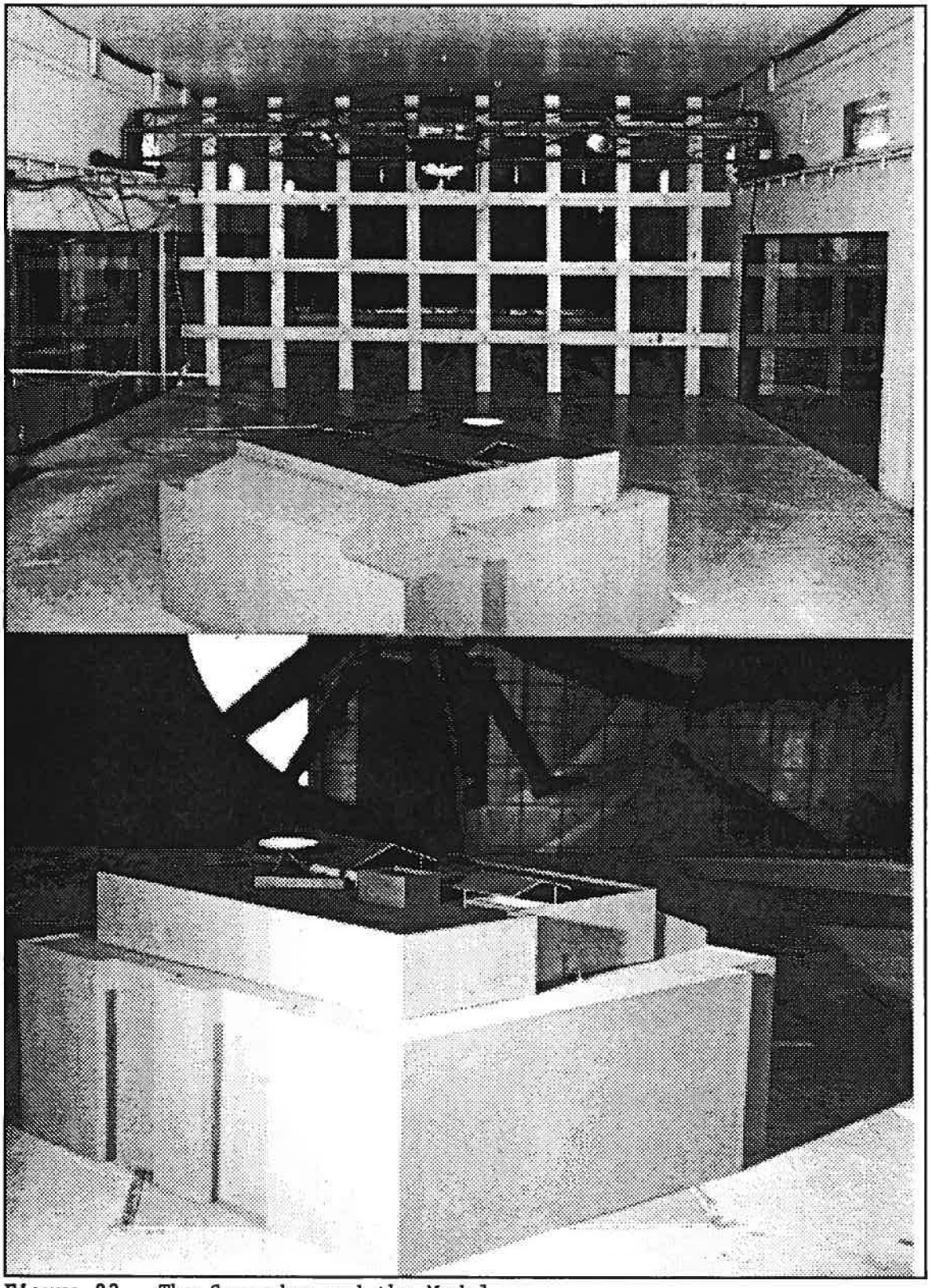

**Figure 23** The Spreader and the Model

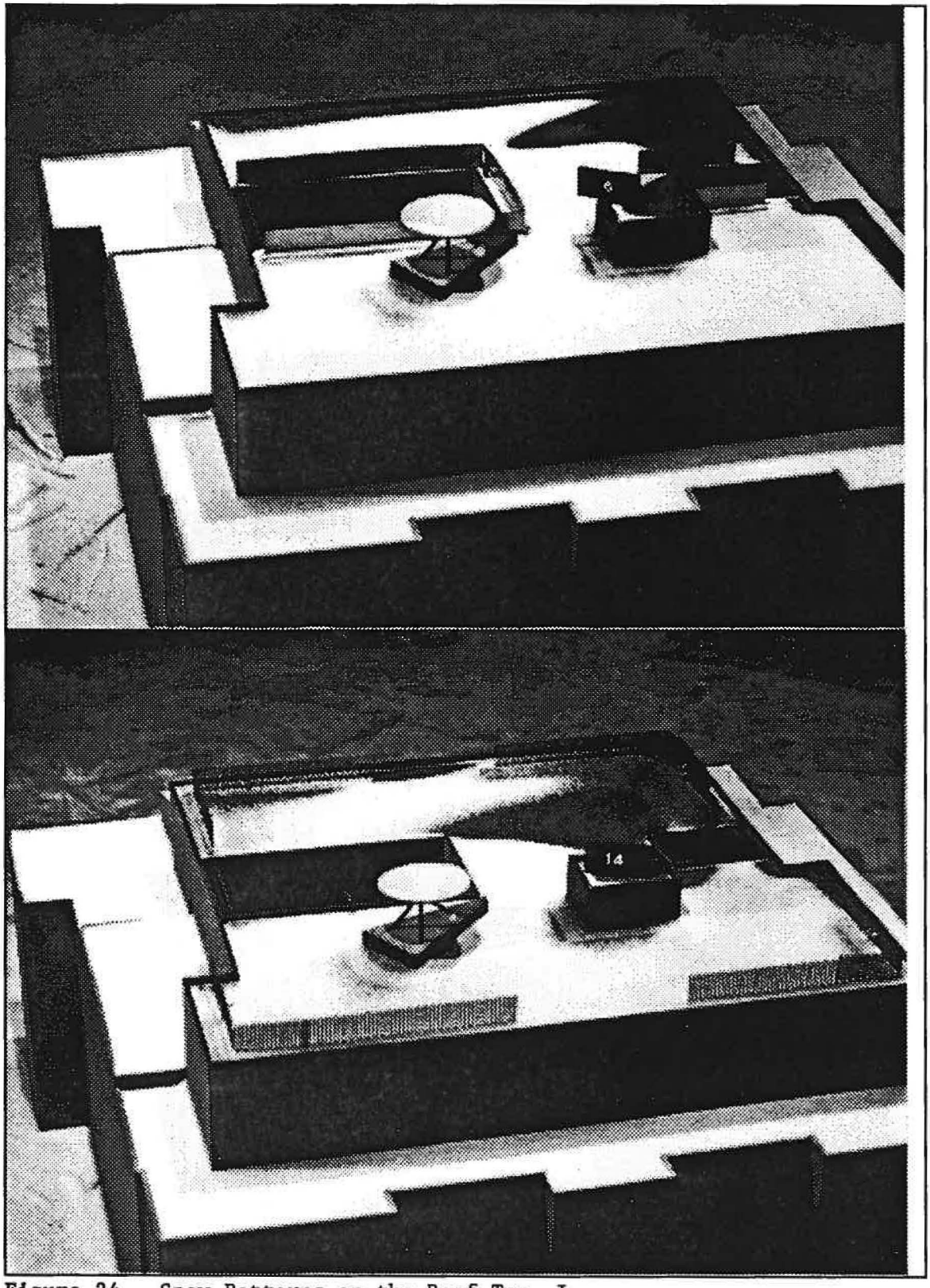


**Figure 24** Snow Patterns on the Roof Top, I

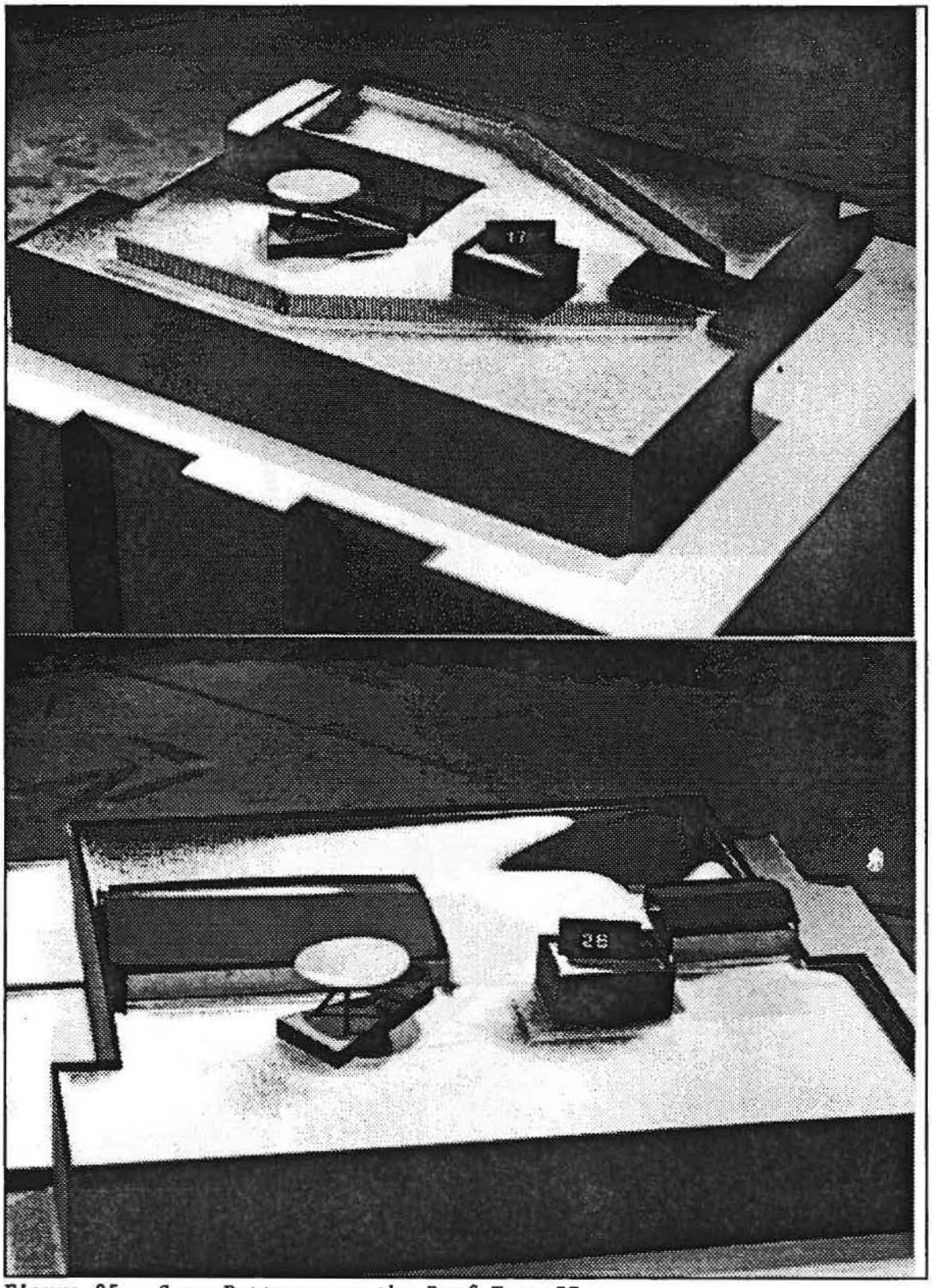

**Figure 25** Snow Patterns on the Roof Top, II

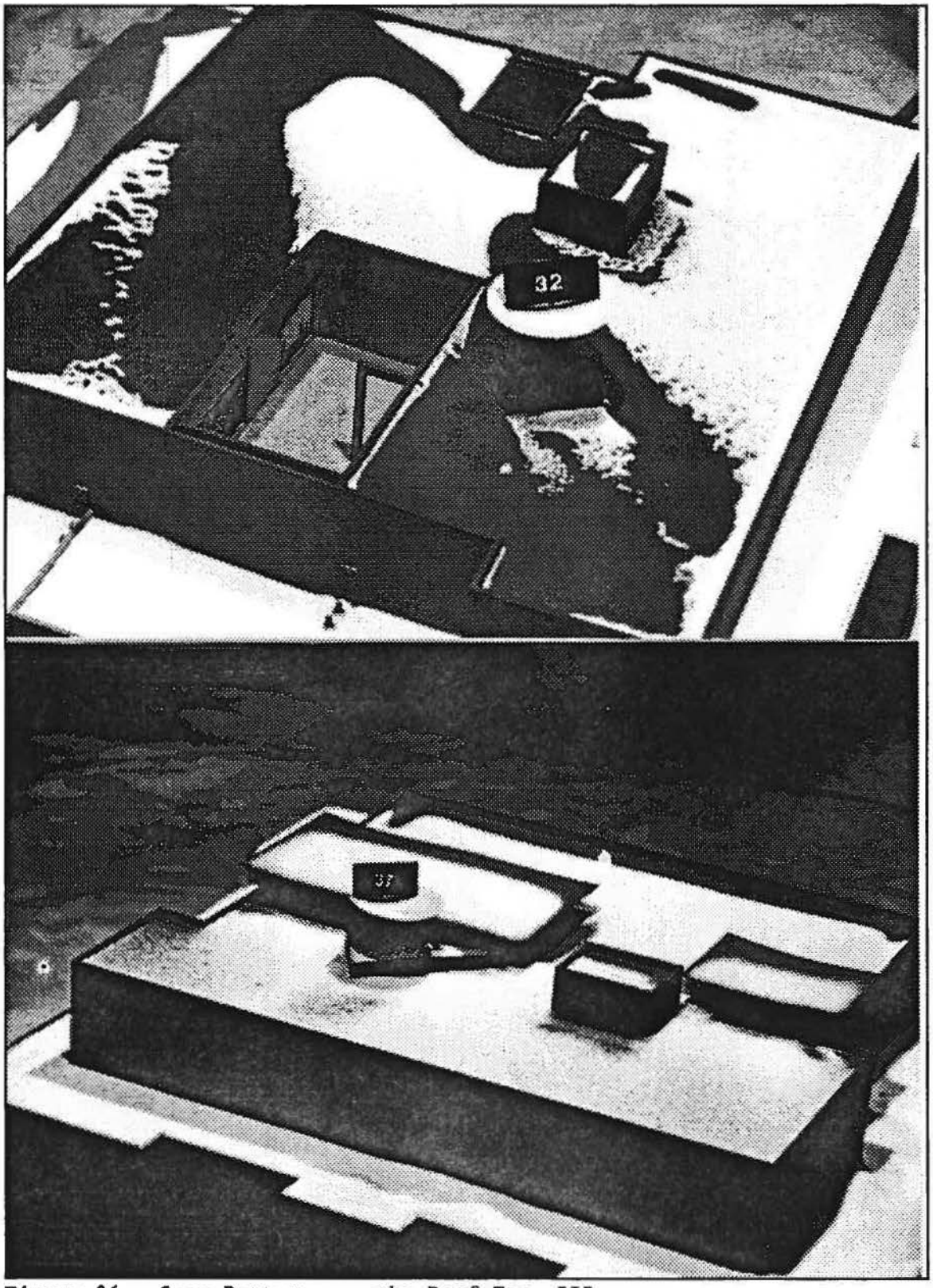


**Figure 26** Snow Patterns on the Roof Top, III

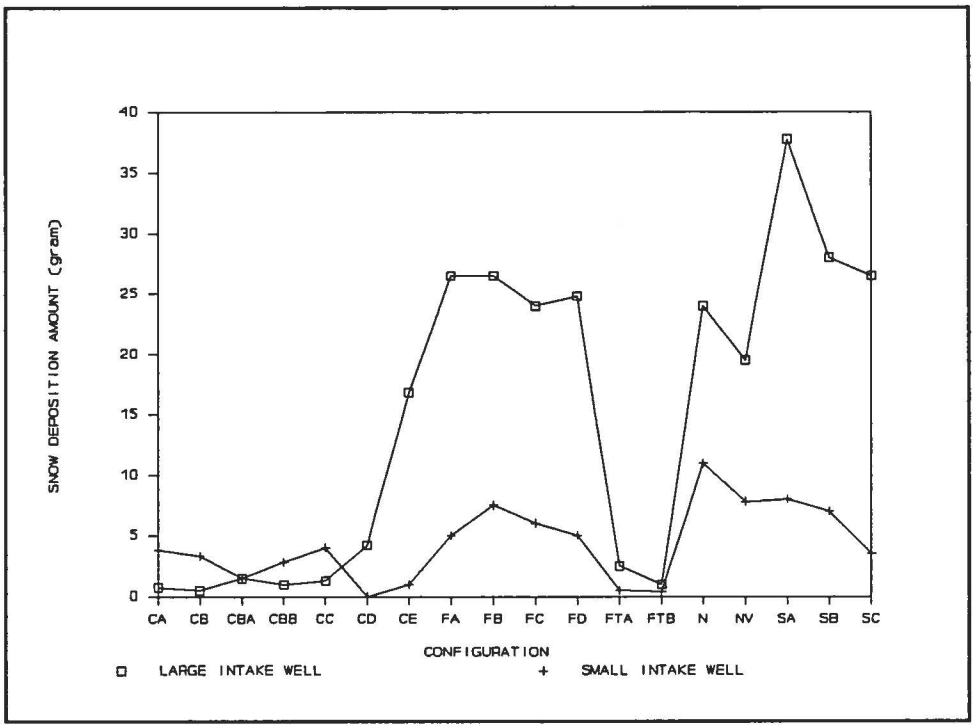


**Figure 27** Snow Deposition Rate for N Wind Direction

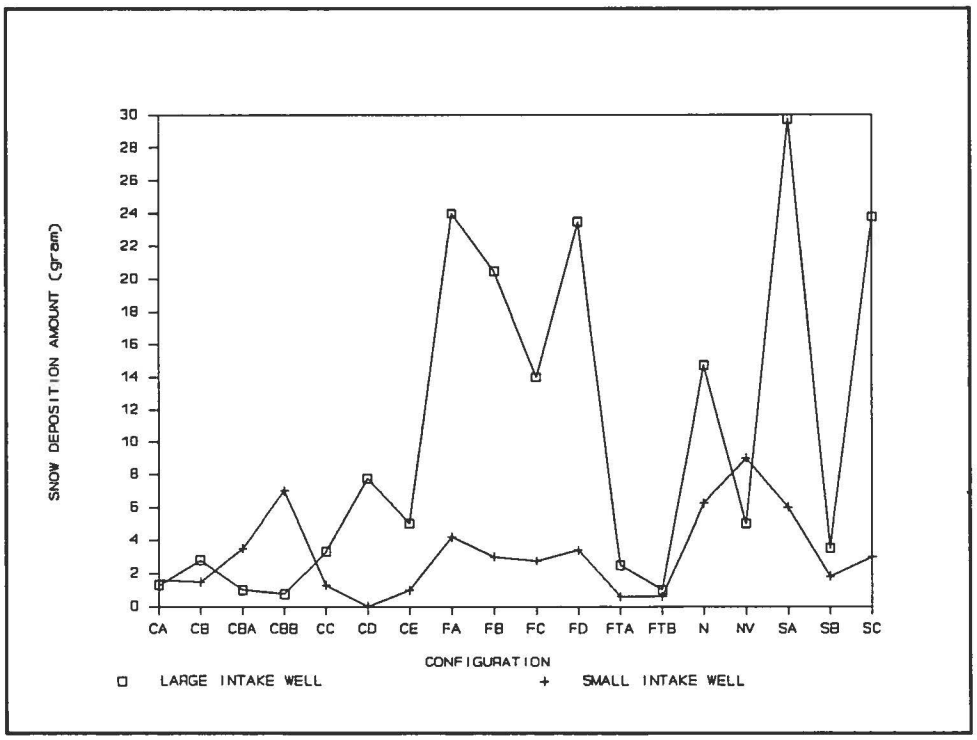


**Figure 28** Snow Deposition Rate for NE Wind Direction

# APPENDIX: WIND-TUNNEL MODELING OF ATMOSPHERIC SITUATIONS

To obtain a predictive model for a snowdrifting problem, one must quantify the pertinent physical variables and parameters into a logical expression that determines their inter-relationships. This task is achieved implicitly for processes occurring in the atmospheric boundary layer by the formulation of the equations of conservation of mass, momentum and energy. These equations with site and source conditions and associated constitutive relations are highly descriptive of the actual physical interrelationship of the various independent variables (space and time) and dependent variables (velocity, pressure, density, etc.).

These generalized conservation statements subject to the typical boundary conditions of atmospheric flow are too complex to be solved by present analytical or numerical techniques. It is also unlikely that one could create a physical model for which exact similarity exists for all the dependent variables over all the scales of motion present in the atmosphere. Thus, one must resort to various degrees of approximation to obtain a predictive model. At present, purely analytical or numerical solutions of boundary layer, wake, and snowdrifting are unavailable because of the classical problem of turbulent closure (Hinze, 1975). However, boundary layer wind tunnels are capable of physically modeling snowdrift processes in the atmosphere under certain restrictions. These restrictions are discussed in the next sections.

## A.1 FLUID MODELING OF THE ATMOSPHERIC BOUNDARY LAYER

The atmospheric boundary layer is that portion of the atmosphere extending from ground level to a height of approximately 1000 meters within which the major exchanges of mass, momentum, and heat occur. This region of the atmosphere is described mathematically by statements of conservation of mass, momentum and energy (Cermak, 1975). The mathematical requirements for rigid laboratory/atmospheric-flow similarity may be obtained by fractional analysis of these governing equations (Kline, 1965). This methodology scales the pertinent dependent and independent variables by size and then casts the equations into dimensionless form by dividing by one of the coefficients (the inertial terms in this case). Performing these operations on such dimensional equations yields dimensionless parameters commonly known as:

| | | | |
|---|---|---|---|
| Reynolds number | $Re = (UL/\nu)_r$ | = | $\frac{\text{Inertial Force}}{\text{Viscous Force}}$ |
| Bulk Richardson number | $Ri = [(Lg\Delta T/T)/U^2]_r$ | = | $\frac{\text{Gravitational Force}}{\text{Inertial Force}}$ |
| Rossby number | $Ro = (U/L\Omega)_r$ | = | $\frac{\text{Inertial Force}}{\text{Coriolis Force}}$ |

Prandtl number $\quad Pr = [\nu/(\kappa/\rho C_p)]_r \quad = \quad \dfrac{\text{Viscous Diffusivity}}{\text{Thermal Diffusivity}}$

Eckert number $\quad Ec = [U^2/C_p\Delta T]_r$

**A.1.1 Exact Similarity**

For exact similarity between flows which are described by the same set of equations, each of these dimensionless parameters must be equal for both flow systems. There must also be similarity between the surface-boundary conditions and the approach flow wind field. Surface-boundary condition similarity requires equivalence of the following features:

a. Surface-roughness distributions,
b. Topographic relief, and
c. Surface-temperature distribution.

If all the foregoing requirements are met simultaneously, all atmospheric scales of motion ranging from micro- to mesoscale could be simulated within the same flow field. However, all of the requirements cannot be satisfied simultaneously by existing laboratory facilities; thus, a partial or approximate simulation must be used. This limitation requires that atmospheric simulation for plume dispersion must be designed to simulate most accurately those scales of motion which are of greatest significance for the transport and dispersion of plumes.

**A.1.2 Partial Simulation of the Atmospheric Boundary Layer**

For many fluid modeling situations several of the aforementioned parameters are unnecessarily restrictive and may be relaxed without causing a significant loss in similarity between model and field fluid flow. The Rossby number magnitude controls the extent to which the mean wind direction changes with height. The effect of Coriolis-force-driven lateral wind shear on wind flow is only significant when heights are of the same order of magnitude as the boundary layer height. The Eckert number (in air $Ec = 0.4\ Ma^2\ (T_r/\Delta T_r)$, where Ma is the Mach number) is the ratio of energy dissipation to the convection of thermal energy. Both in the atmosphere and the laboratory flow, the wind velocities and temperature differences are such that the Eckert number is very small; hence, it is neglected. Prandtl number equality guarantees equivalent rates of momentum and heat transport. Since air is the working fluid in both the atmosphere and the laboratory, Prandtl number equality is always maintained.

The approach flow Richardson number (Ri) and Reynolds number (Re) determine the kinematic and dynamic structure of turbulent flow within a boundary layer. This influence is apparent in the variations that occur in the spectral distribution of turbulent kinetic energies with changing Ri and changing Re.

## The Reynolds Number

Re equality implies $U_m = (L_p/L_m)U_p$. Re equality at a significantly reduced length scale would cause the model's flow velocity to be above sonic; hence, its equality must be distorted. A reduced Re changes only the higher frequency portion of an Eulerian-type description of the spectral energy distribution. Unfortunately, there is no precise definition as to which portion of an Eulerian Spectrum is dominant in dispersing ground-level or elevated plumes over moderate travel distances.

Most investigators use a minimum Reynolds number requirement based on rough-walled pipe measurements; i.e., $Re = u_* z_o/\nu > 2.5$, where $u_*$, the friction velocity, and $z_o$, the roughness length, are derived from a log-linear fit to a measured mean velocity profile. The value 2.5 is an empirically determined constant. At Re below 2.5, it is observed that the mean velocity profiles in turbulent pipe flow lose similarity in shape and deviate from the universal curve of a rough wall turbulent boundary layer. For Re above 2.5, it is observed that the surface drag coefficient (and thus the normalized mean velocity profile) is invariant with respect to increasing Re. For Re between 0.11 and 2.5, the velocity profiles are characteristic of smooth wall turbulent boundary layers. For values below 0.11, the growth of a laminar sublayer on the wall is observed to increase with decreasing Re.

Extrapolation of results from pipe flow measurement to flat plate boundary layers may cause a shift in the magnitude of the minimum Re requirement, but it is generally felt that this shift is small. Precise similarity in the universal form of mean wind shear may be necessary for invariance with respect to the surface drag coefficient, but this does not necessitate that precise similarity must exist for the invariance of the wind field and dispersion. It is the distribution of turbulent velocities which has the greatest effect on the wind field and dispersion. It is the mean wind shear, however, which generates the turbulent velocities. It is possible that the specification of a minimum Re of 2.5 is overly conservative. The criteria, $Re > 2.5$, for example, is not applicable for flow over complex terrain or building clusters.

## The Richardson Number

Although most wind-tunnel investigations are conducted with neutrally stratified boundary layers, there are circumstances when the stratification of the atmosphere must be considered. In particular, air pollution and dispersion problems are often critical during stratified conditions. Unstable stratification may be expected to mitigate hazards by accelerating plume dilution, whereas stable stratification may permit high concentrations to persist. The stability state of the atmosphere is typically characterized by the Richardson number.

The atmospheric gradient Richardson number can be computed from averaged quantities through the equation

$$Ri = g/T\ (\Gamma_d - \Gamma)\ [1 + 0.07/B]\ [(\partial u/\partial z)^2 + (\partial v/\partial z)^2]$$

where $\Gamma$ and $\Gamma_d$ are the actual and dry adiabatic potential temperature lapse rates, and $B = [C_p(T_2-T_1)]/[(Z_2-Z_1)(Q_2-Q_1)]$ is the Bowen ratio of sensible to latent heat flux at the surface. The Ri number can be taken to represent the ratio of the relative importance of convective and mechanical turbulence. Negative Ri numbers of large value indicate strong convection and weak mechanical turbulence; zero Ri numbers imply purely mechanical turbulence. Positive Ri numbers less than some critical value, $Ri_{critical}$, suggest the presence of mechanical turbulence damped by the density-induced buoyancy forces; for larger positive Ri numbers, turbulence essentially disappears, since the stratification overpowers production by wind shear. The critical Richardson number has a value near 0.25.

### A.1.3 Performance of Prior Fluid Modeling Experiments

Meroney et al. (1978) summarized experimental data available from field and laboratory studies for neutral airflow over hills, ridges, and escarpments. Wind-tunnel model measurements were performed to study the influence of topography profile, surface roughness and stratification on the suitability of various combinations of these variables. Detailed tables of velocity, turbulence intensity, pressure, spectra, etc., were prepared to guide numerical model design and experimental rule of thumb restrictions. Cases included hill slopes from 1:2 to 1:20, neutral and stratified flows, two- and three-dimensional symmetric ridges, six alternate hill and escarpment shapes, and a variety of windward versus leeward slope combinations to evaluate ridge separation characteristics. The laboratory data were validated by comparison with field measurements for flow in the Rakaia Gorge, New Zealand, and over Kahuku Point, Oahu, Hawaii, (Meroney et al., 1978; Chien, Meroney and Sandborn, 1979).

Local heating and cooling of coastline or hill surfaces are the driving mechanisms for sea-land breezes, and anabatic and katabatic winds which may inhibit or enhance airflow over the land surface. Early laboratory work includes simulations of urban heat islands by Yamada and Meroney (1971) and Sethuraman and Cermak (1973), simulation of flow and dispersion at shoreline sites by Meroney et al. (1975a), and simulation of dispersion effects of heat rejected from large industrial complexes by Meroney et al. (1975b).

Meroney (1980) compared three model/field investigations of flow over complex terrain, suggested performance envelopes for realizable modeling in complex terrain, and discussed recent laboratory studies which provide data for valley drainage flow situations. Not all of the model/field comparison experiments performed in the past were successful. Many early studies had model approach flow velocity exponents near zero, were modeled as neutral flows when the field observed strong stratification effects, or simulated unrealistic boundary layer depths, integral scales, or turbulence intensities which did not match their atmospheric counterpart. But few studies claimed unreasonable correlation, and some were strongly self-critical. Nonetheless, most studies accomplished their prestated limited objectives. It would appear

that the simulation hypothesis developed in the last few years is appropriate for physical modeling of flow over complex terrain when appropriate care is taken to simulate the approach flow conditions and to maintain simulation parameters equal between model and prototype.

Arya and Plate (1969), Arya (1975) performed velocity, temperature, and turbulence measurements in the lowest 15 percent of a 70 cm deep boundary layer over a smooth surface, where conditions ranged from unstable to moderately stable ($-0.3 < z/L_{mo} < 0.3$). Free stream flow speeds varied from 3 to 9 m/s, and temperature differences were about 40°C across the boundary layer. Cermak, Shrivastava and Poreh (1983) reported mean velocity and turbulence measurements made for a variety of simulated atmospheric boundary layers over different surface roughness. Free stream flow speeds varied from 2.4 to 3.0 m/s and temperature differences were from 150°C to -80°C across the boundary layer. Poreh and Cermak (1984) reproduced unstable lapse conditions including mixed layers and elevated inversions. They reproduced the characteristics of convective boundary layer turbulence measured in the atmosphere.

Diffusion studies made by Chaudhry and Meroney (1973) in stable boundary layers investigated previously by Arya (1969) have shown agreement of experimental results with Lagrangian similarity theory. Horst (1979) tested Lagrangian similarity predictions of crosswind-integrated ground concentration against the Prairie Grass diffusion experiment (Barad, 1958) and an experiment at Idaho Falls (Islitzer and Dumbauld, 1963). He reported good agreement for all stabilities at distances $x/z_o$ out to $2*10^5$. Poreh and Cermak (1984, 1985) released plumes in their modeled mixing layer. Their plumes exhibited the plume lofting typical of ground sources and the descent typical of elevated sources, predicted from water tank experiments by Willis and Deardorff (1974, 1976, 1978) and numerically by Lamb (1982).

Staff at the Fluid Mechanics Laboratory at the Ecole Centrale de Lyon have studied unstable wind-tunnel boundary layers and compared them with the atmospheric boundary layer (Schon and Mery, 1971). Flow speeds were typically 2 to 4 m/s and the floor temperature was maintained 50°C above ambient. Comparisons with the Kansas data (Haugen et al., 1971) were quite satisfactory, but longitudinal turbulence intensities exhibited a slight Reynolds number dependence, and spectral energy was too low in the high frequency portions of the spectra. The most unstable flow they studied had a Monin-Obukhov scale length of about -1 m at model scales, or -500 to -1000 when scaled to the atmosphere.

## A.2 PHYSICAL MODELING OF BLUFF BODY AERODYNAMICS

The interaction of an approach wind field with bluff bodies or structures constructed on the earth's surface is broadly termed "Building Aerodynamics." In a review article on this subject, Meroney (1982) discusses the character of bluff body flow about rectangular buildings and cylindrical cooling towers. Defects in velocity profiles can easily

persist from 10 to 15 building heights downwind. Field and laboratory measurements of plume dispersion about the Rancho Seco Nuclear Power Station in Sacramento, California, confirm that cooling tower wake effects persist for significant downwind distances under a variety of stratification conditions (Allwine, Meroney and Peterka, 1978; Kothari, Meroney and Bouwmeester, 1981).

### A.2.1 Simulation Criteria

Often atmospheric turbulence may cause only weak effects compared to the turbulence generated by buildings, obstacles, and terrain. Yet the magnitude of the perturbations depends upon the incident flow turbulence scale and intensity, details of the obstacle shape and surface roughness, and size of the obstacle compared to the boundary layer depth. Geometrical scaling implies that the ratio of the building height to length scale must be matched and, of course, that all other building length scales be reduced to this same ratio.

Several questions should be considered when modeling flows which include surface obstacles:

a. What size obstacles should be disregarded?
b. What detail or roughness on an obstacle need be included?
c. To what upwind distance should all obstacles be included?
d. At what point does the size of a modeled obstacle become too big for the wind tunnel (i.e., blockage effects)?
e. What is the effect on the flow field of mismatching obstacle and approach flow length scales?
f. What is the minimum allowable model obstruction Reynolds number?

**Obstacle sizes to be disregarded:**

Boundary layer studies of rough surfaces reveal that if protuberances are of a size k, such that $u_*k/\nu < 5$, they will have little effect on the flow in a turbulent boundary layer. Thus, assuming a laboratory wind speed of 1 m/s and a typical friction coefficient $C_f/2 = (u_*/u)^2 = 0.0025$, obstacles of size less than 2 mm would go unnoticed.

**Required obstacle surface detail or roughness:**

Another question that always arises is "How much detail is required for the building or obstacle model? The answer is, of course, dependent upon the size of the protuberance compared to the plume and the dominant eddies of mixing. If the obstruction is large enough to modify the separated wake over the main obstacle, then it must be included. Often an equivalent obstacle surface roughness suffices. Snyder (1981) concludes a generic surface roughness criterion might be $u_*k/\nu > 20$. For a 1 m/s laboratory flow this results in model roughness elements equal to about 6 mm. But since the exterior flow is usually highly turbulent, the body typically includes a highly unsteady wake, and the $u_*$ value to be used should be that acting on the building surface, rather than that of the approach flow. Hence, even this roughness may be unnecessarily large.

**Upstream fetch to be modeled:**

Suppose there is another building, tree line, fence, cooling tower, or obstacle some distance, s, upstream of a meteorological measurement location; is it necessary to include this obstacle in the wind-tunnel model? Hunt (1974) showed that the velocity deficit in the wakes of cubes and cylinders is given approximately by:

$$DU_{mx}/U(h) = A\ (s/h)\text{-}3/2$$

downwind of the separation bubble, where $DU_{mx}$ is the maximum mean velocity deficit created by the obstacle, h is the height of the obstacle, S is the distance downstream of the obstacle, and A is a constant dependent upon the obstacle shape, orientation, boundary layer thickness, etc. Typically, A = 2.5, but it may range from 1.5 to 5.0. If we desire that the velocity at the spill site be within 3 percent of its undisturbed value, Snyder (1981) recommends that any upstream obstacle as high as s/20 be included upstream in the model of the spill site. If the obstacle's width is much greater than its height (for example, a fence or ridge), one should include it in the physical model if its height is greater than s/100.

**Blockage effects:**

Because of the influence of wind-tunnel walls on the behavior of the flow past models, it is desirable to use small models or big tunnels, or both. On the other hand, larger models are not only easier to work with, but they may be needed for similarity reasons to achieve large enough Reynolds numbers. It is possible to identify three different types of effects of wind-tunnel constraints. The first is the simple "solid blockage" effect which arises because the fluid stream is unable to expand laterally as it normally would in unconfined flow. The second effect, called "wake blockage", results because the accelerated flow between an obstacle and the tunnel walls continues to "pinch" the wake flow region and reduce its normal lateral rate of growth. The third effect is produced by the growth of boundary layers on the tunnel walls which produce "wall boundary interference." Tunnel blockage can cause separation and reattachment locations to vary, produce higher velocities, larger wake turbulence, and modify the dispersion patterns in the vicinity of obstructions.

The ratio of the cross-sectional area of a model obstacle to that of the tunnel is called the "blockage ratio", BR. Mass continuity produces an average velocity speed-up of S = BR/(1-BR). Although wind tunnels with adjustable ceilings can compensate to some extent by raising the roof locally; this is not a perfect solution to the problem. Measurements on building and cooling tower models placed in different size wind-tunnel test sections reveal major changes in the character of pressure distributions, separation, and wake growth in the presence of flow restricted by wind-tunnel side walls (Farell et al., 1977).

Blockage corrections, which are conventionally applied in aeronautical tunnels, cannot usually be applied to the typical asymmetric model configuration placed against the wall of a meteorological wind tunnel (Ranga Raju and Singh, 1976). Conventional wisdom now suggests the "rule of thumb" that blockage ratios greater than five percent should be avoided.

**Simulation of the flow over sharp-edged obstacles:**

A number of authors have discussed flow studies about simple cubical or rectangular sharp-edged obstacles. An extensive review about such flow fields and the subsequent character of diffusion near obstacles has been provided by Hosker (1984). Peterka, Meroney and Kothari (1985) describe typical flow deviations which result from the presence of a sharp-edged building.

Consider the main features of the flow around a sharp-edged building. Typically, when the approach flow is normal to the building face, the flow separates from the ground upwind of the building and produces a "horseshoe"-shaped vortex which wraps around the base of the building. The surface streamline reattaches on the front of the building, and fluid parcels move up and down the building's forward face. An elevated streamline flows over the obstacle, dips down behind, and stagnates on the surface at the end of the recirculating cavity immediately downwind of the building. Sometimes separation streamlines from the forward building edges reattach to the same face, yet in other cases the streamlines enter the downwind cavity and mingle with the other recirculating fluid. Air which enters the cavity departs through turbulent mixing across the dividing streamlines, mingles with downwind-pointing vortices and is ejected laterally out of the cavity, or leaves suddenly during an exhalation when the entire cavity appears to collapse and then reform.

When a building is oriented obliquely to the wind, flow over the front side walls does not separate, but strong recirculation occurs on the downwind faces. Flow over the roof often produces counter-rotating "delta-wing" vortices which increase mixing over the top and in the wake of the building. These vortices can cause reattachment of the flow in the middle of the roof and serious plume downwash in the near wake. Other features of the flow near the building include vertical vortices produced by the vertical corners of the building.

Golden (1961) measured the concentration patterns above the roof of model cubes in a wind tunnel. Two sizes of cubes were used to vary the Reynolds number from 1000 to 94,000. The concentration isopleths in the fluid above the cube roof showed only slight variations over the entire range of Reynolds numbers studied. The maximum concentration on the roof itself was found to vary strongly with Reynolds numbers less than 11,000, but to be invariant with Reynolds numbers between 11,000 and 94,000. Frequently, modelers quote Golden's experiments as justification for presuming dispersion invariance when obstacle Reynolds numbers exceed 11,000. However, Golden's "11,000 rule" is limited to the measurement of

concentrations at only one point on the roof of smooth-walled cubes placed in a uniform approach flow of very low turbulent intensity. It is probably quite conservative because the shear and high turbulence in a simulated atmospheric boundary layer are likely to further reduce the critical Reynolds number. Indeed, Halitsky (1968) observed that for dispersion in the wake region, no change in isoconcentration isopleths from passive gas releases was found to occur for values of Reynolds number as low as 3300.

Flow around sharp-edged obstacles will remain kinematically similar at very low Reynolds numbers. Wake width variation will be minimal, and obstacle generated turbulence scales and intensity will only vary slowly as Reynolds number decreases. Gas clouds dispersing in this environment will remain similar at very low model speeds.

**Simulation of flow over rounded obstacles:**

Flow around a smooth cylinder is Reynolds number dependent. This dependence reflects changes in the nature of the boundary layer that forms over the cylinder and its behavior in the vicinity of the flow separation. At low Reynolds numbers, the boundary layer is laminar, and separation occurs easily under the influence of even modest positive pressure gradients. At higher Reynolds numbers, the boundary layer becomes turbulent and flow separation is delayed; i.e., the flow can move farther along a curved surface without separation. At prototype scales, obstacles are large enough that only turbulent separation occurs. However, model flows are usually at such low Reynolds numbers that the local boundary layer growing over a curved surface would be laminar. Most modelers attempt the reproduction of full- scale similarity around curved surfaces by artificially roughening the model surface to force transition to turbulence in these laminar boundary layers. This can be done by providing the surface with special (or artificial) roughness elements, for example, sandpaper, thin wires, or grooves. The height of the roughness, k, should be such that $Uk/\nu > 400$ and $k/R < 0.01$, where U is the mean wind speed at obstacle height, and R is the characteristic obstacle radius of curvature. Szechenyi (1975) studied flows about rough circular cylinders and determined that as Reynolds number decreases, roughening the surface becomes less effective. Fage and Warsap (1929) considered the effect of increasing the surface roughness of cylinders on their drag coefficient. Eventually, even ridiculously large roughness is ineffective.

Niemann and Ruhwedel (1980) compared pressures and forces about a 1:333 scale model to a full-scale hyperbolic cooling tower shell. They roughened their model with vertical ribs of height 0.09 mm and width 0.77 mm, producing a roughness coefficient of $k/2R = 0.0006$ and roughness Reynolds number, $Re_k > 270$. They found meridional forces on the cooling tower model and prototype were similar. Model Reynolds numbers were between $4.5*10^5$ and $6.0*10^5$, and this corresponding to $U_m > 45$ m/s. But again these speeds are much higher than is appropriate for current measurements.

Halitsky et al. (1963) examined dispersion about a smooth-model nuclear reactor containment building (a hemisphere fitted on a vertical cylinder) and found a critical Reynolds number greater than 79,000. (Yet this critical Reynolds number was for flow very close to the vessel wall. The behavior of concentration isopleths further downwind is likely to be less Reynolds number dependent.)

Although the details of fluid motions around rounded obstacles vary significantly with Reynolds number, the gross features of the flow do not change. Even small models at low wind speeds will produce horseshoe-shaped ground vortices, elevated pairs, and regular vortex shedding. If the internal boundary layer over the obstacle is laminar, then the wake region will be broader and less intense.

### A.2.2 Performance of Prior Fluid Modeling Experiments

A number of studies have been performed in the Colorado State University Fluid Dynamics and Diffusion Laboratory to establish the effect of buildings and meteorological masts on flow fields. Hatcher et al. (1977) examined flow and dispersion in stratified flow downwind of the Experimental Organic Cooled Reactor, Idaho Falls; Allwine et al. (1978) studied the Rancho Seco Reactor, Sacramento; Kothari et al. (1981) studied the Duane Arnold Energy Center, Iowa. In each case field measurements were compared to laboratory measurements with good agreement. Specific effects of the structure of a meteorological mast on instrumentation response were reported by Hsi and Cermak (1965).

## A.3 PHYSICAL MODELING OF SNOW MOVEMENT

The problem of drifting snow in the colder populated regions of the world has long been a difficult one, both in terms of predicting drift patterns and in establishing possible control by means of vegetation, snow fences, or other obstructive devices. A host of snow-drift problems exist in connection with highways, railroads, access to buildings and animal protection. Experimentally, it is time consuming and often unrewarding to study snow drift patterns in the field, since control of weather conditions is not possible and measurements are difficult. Thus, modeling techniques can be very useful if valid predictions can be made from models. In the laboratory conditions can be carefully controlled, and many different situations can be simulated in a short time with much less expense than that incurred with full-scale experiments.

The value of wind tunnel testing to determine snow-drift characteristics has been recognized for years, but relatively few studies have been conducted. Experiments which have been carried out related to highways (snow fences) include those of Becker (1944), Nokkentved (1940), and Finney (1937). Studies related to building proximity include Gerdel and Strom (1961), Strom et al. (1962), and Threakston (1970). An early set of experiments was conducted by Woodruff and Zingg (1952) on windbreaks. Studies to estimate eolian movement of sand on the surface

of Mars have been conducted at Iowa State University Wind Tunnel Laboratory and at the NASA Ames Research Center (1974, 1979a, 1979b, 1980a, 1980b, 1981, 1989). Gray and Male (1981) have edited a comprehensive text on the management of snow. Snow control by conventional porous fences has been optimized by Tabler (1981a) and the evaluation of snow movement by Tabler (1981b). Recently, snow control by less-familiar blower devices, vortex fences, or baffles were examined (Meroney and Meroney, 1988).

### A.3.1 Simulation Requirement

There are three main requirements in model testing: (1) geometric similarity, (2) kinematic similarity, and (3) dynamic similarity.

Geometric similarity

Geometric similarity requires that ratios of corresponding linear dimensions be equal. In an undistorted model these ratios do not change with direction. If L is a linear dimension and the subscripts p and m refer to the prototype and model, geometric similarity requires

$$L_m / L_p = \text{constants}.$$

This constant is the selected scale such as 1:50 or 1:150.

During simulation of drifting snow strict application of above equation to particle size produces exceedingly small simulant particles. Hence, geometric similarity is normally preserved in the model for all dimensions except the size of the particles. If the drifts can be duplicated without meeting the geometrical similarity requirement for particle size, the problem of simulation of snow transport is solved.

Kinematic similarity

Kinematic similarity requires that the ratio of velocities and directions at corresponding points of two geometrically similar systems be equal. That is, the velocities in nature will be reduced in the model by a certain ratio. If V is the velocity, the kinematic similarity can be expressed as

$$V_m / V_p = \text{constant}.$$

One of the results of kinematic similarity is that the coefficient of restitution of the snow particles and the simulate material should be equal.

Kinematic similarity also requires duplication of the boundary layer and turbulence structure. Boundary layer threshold characteristics of the particles. Turbulent fluctuations and eddies affect the paths of the particles.

Dynamic similarity

Dynamic similarity requires that the ratios of forces at corresponding points of geometrically similar systems be equal. Dynamic similarity provides similar motions and paths for fluid and mass particles in the model. Dynamic similarity can be formulated as

$$F_m / F_p = \text{constant},$$

in which F is the force.

Dynamic similarity is very important in simulation of drifting snow. It will be used to duplicate the paths and the threshold characteristics of the particles. Given dynamic similarity and geometric similarity then kinematic similarity is guaranteed by Newton's laws of motion.

### A.3.2 Simulation Criteria

Based on dimensional analysis the following list of similitude parameters useful in the description of saltation phenomena, can be identified:

| | | |
|---|---|---|
| 1. | $D_p/L$ | particle diameter - length ratio |
| 2. | $U(h)/U_f$ | reference to particle terminal speed ratio |
| 3. | $[U(h)]^2/gL$ | Froude number |
| 4. | e | coefficient of restitution |
| 5. | $L_m/L_p$ | topographic geometric similarity |
| 6. | $z_o/L$ | roughness similitude |
| 7. | $z_o'/L$ | roughness similitude in saltation |
| 8. | $h/L$ | reference height ratio |
| 9. | $z_o/L^*$ | stability parameter |
| 10. | $\lambda/L$ | ripple length ratio |
| 11. | $U_f/U_{*t}$ | particle property similitude |
| 12. | $U_{*t}D_p/\nu$ | particle friction Reynolds number |
| 13. | $U(h)L/\nu$ | flow Reynolds number |
| 14. | $U_*/U_{*t}$ | friction speed ratio |
| 15. | $\rho/\rho_p$ | density ratio |
| 16. | $U(h)t/L$ | time scale |

It is impossible to satisfy all terms of Parameters 1 to 15 simultaneously (Parameter 16 is a prediction term). Different parameters were proposed by different researchers. The first four of these parameters were suggested by Gerdel and Strom (1962) as the scaling parameters of primary importance in the modeling of accumulation of wind-driven snow. Odar (1965) added Parameters 2, 3, 11, 15. Kind (1976) considered Parameter 2, 3, 11 and a minimum Reynolds number requirement as the only important parameters. Isyumov(1971) recommended Parameters 2, 3, 11.

Nevertheless, two parameters which were favored by most of the researchers:

1. The Froude number $U^2/ gL$ ;
2. The ratio of falling velocity and threshold velocity $U_f / U_{*t}$.

Unfortunately the Froude number cannot always be satisfied, since $U_m = U(L_m/L_p)^{\frac{1}{2}}$. If the length scale $L_p / L_m$ is large, $U_m$ may be too small and the tunnel speed may be below any threshold speed. It may also be so low that a minimum Reynolds number requirement could not be satisfied.

Anno (1989) recently argued that the Froude number is unsuitable as a similitude parameter for the modeling of snowdrifts.

He argues that if Froude scaling holds for the modeling of snowdrift, the velocity scaling must be estimated as

$$(U_p/U_m)^2 = (U_{*p}/U_{*m})^2 = L_p/L_m.$$

However, since the threshold friction velocity has the same dimensions as friction velocity, the following relation between them must hold in the modeling experiment

$$U_{*p}/U_{*m} = U_{*pt}/U_{*mt},$$

which leads to the following

$$U_{*pt}/U_{*mt} = L_p/L_m.$$

Thus, the ratio of the threshold friction velocity between the model and prototype must depend only on the geometric scale. This result contradicts the broadly accepted conclusion that the threshold friction velocity for snow transport is determined not only by size but also by temperature, humidity, history of snow, density and shape of particles.

Following the arguments of Anno (1989), only the fall velocity to threshold friction velocity will be constrained during these tests.